and 5′-tgcgtacctaggttaagaagagttttccctcaattttctt-3′, which contain NheI and BamHI sites, respectively. The PCR product was cloned into the corresponding sites of the pET-28 a(+) vector (Novagen) to obtain the expression vector pET-LRPPRC, which produces N-terminal His-tag-fused LRPPRC (His-LRPPRC). The *E. coli* rosetta (DE3) strain was transformed with pET-LRPPRC and cultured in LB media containing 50 μg/ml kanamycin and 30 μg/ml chloramphenicol. Protein expression was induced by adding lactose to a final concentration of 2% and the cells were grown at 25°C for 20 h. Cells were harvested and suspended in buffer C [50 mM HEPES–KOH (pH 7.6), 100 mM KCl, 10 mM $MgCl_2$ and 7 mM β-mercaptoethanol], followed by sonication on ice. Cell lysates were cleared by ultracentrifugation at 100 000*g* for 60 min. The supernatant was loaded onto a nickel-charged HiTrap chelating column (GE Healthcare). After washing off unbound proteins with buffer C, recombinant proteins were eluted with a 50 ml linear gradient from 0 to 500 mM imidazole in buffer C. Fractions containing the recombinant proteins, which were visualized by SDS–PAGE followed by CBB staining, were pooled and dialyzed overnight against buffer D [20 mM Tris–HCl (pH 6.8), 100 mM NaCl, 4 mM $MgCl_2$ and 1 mM DTT]. The His-LRPPRC was then loaded onto a Mono Q 5/50 column (GE Healthcare). After washing off unbound proteins with buffer E [20 mM Tris–HCl (pH 6.8), 100 mM NaCl, 4 mM $MgCl_2$, 7 mM β-mercaptoethanol], His-LRPPRC was eluted with a 25 ml linear gradient from buffer E to buffer F [20 mM Tris–HCl (pH 6.8), 500 mM NaCl, 4 mM $MgCl_2$ and 7 mM β-mercaptoethanol]. Eluted fractions were analyzed by SDS–PAGE followed by CBB staining. Glycerol was added to the pooled protein fractions to a final concentration of 10%. The concentration of purified His-LRPPRC was determined by the BCA protein assay (Thermo Scientific) using BSA as a standard. HeLa cell total lysates and the purified His-LRPPRC were subjected to SDS–PAGE and analyzed by western blotting using anti-LRPPRC antibody. The copy number of LRPPRC in one HeLa cell was determined by the signal intensity, using the calibration line of the external standards generated by the purified His-LRPPRC.

Relative quantification of mtDNA in HeLa cells

HeLa cells transfected with Luciferase or PNPase siRNAs and grown in 10 cm dishes were trypsinized and collected. Cell pellets were lysed by 1 ml of buffer G [10 mM Tris–HCl (pH 8.0), 1 mM EDTA (pH 8.0), 0.6% SDS and RNase A]. Cell lysates were incubated at 37°C for 1 h. 5 μl of Proteinase K (Roche) was added, and cell lysates were incubated at 55°C for 2 h. Cell lysates were sonicated by Sonifier 450D (Branson) at power 3 for 24 s. Proteins were removed by addition of PCI (Nacalai) followed by 10 min of vortexing and centrifugation. Total DNA was collected by ethanol precipitation. 0.75 μg of total DNA was used for quantitative real-time PCR of mtDNA or 18 S rDNA, using the LightCycler 480 SYBR Green I Master (Roche) on a LightCycler 480 (Roche) according to the manufacturer's instructions. The sequences of the qPCR primers are listed in Supplementary Table S1.

In vitro polyadenylation assay

ΔN39 MTPAP-His expression vector and recombinant protein were obtained as previously described (19). Recombinant LRPPRC protein was obtained as described above. *COX2* and *COX3* mRNA in Figure 5B were made as described above. The DNA templates used for the *in vitro* T7 RNA transcription of the substrate RNAs shown in Figure 5C and D were made by PCR amplification of sections of the *ND1* and *ND4L/4* genes. Double-stranded RNAs in Figure 5C were made by annealing the transcripts, and the double-stranded RNAs were then purified by polyacrylamide gel electrophoresis. Polyadenylation reaction was carried out at 37°C for 30 min. Each reaction contained substrate RNA and recombinant MTPAP protein in 20 μl of reaction buffer, which was composed of 50 mM Tris–HCl (pH 8.0), 40 mM KCl, 0.5 mM $MgCl_2$, 0.1 mM $MnCl_2$, 1 mM DTT, 167 nM α-^{32}P ATP and 0.1 mM cold ATP. In Figure 5B, D and E, LRPPRC protein was added to the reaction and incubated at 37°C for 10 min, before the addition of α-^{32}P ATP and MTPAP protein. RNA was purified using TRI Pure (Roche) and ethanol precipitation and was resolved by denaturing PAGE. The RNA was visualized by exposing the gel to FLA-7000 (Fujifilm). All oligo-DNAs are listed in Supplementary Table S1.

RESULTS

Absolute quantification of human mitochondrial mRNAs in HeLa cells

In human mitochondria, 10 species of mRNA are generated from a single long precursor H-strand RNA. Differences in the steady-state levels of these 10 mRNAs were analyzed by qRT-PCR (3), by measuring the cDNA numbers of polyA(+) RNAs (4) and by deep sequencing (37). These studies reported only the relative and non-absolute values of mRNAs in human mitochondria. Precise analysis of the concentration or number of each species of mRNA in one cell is needed to obtain a more accurate representation of mRNA metabolism in human mitochondria. Thus, we decided to determine the exact copy numbers of all mitochondrial mRNAs in human HeLa cells. For absolute quantification of each mRNA, *in vitro* transcribed mRNAs were prepared as external standards for qRT-PCR. In addition, the extraction efficiency of mRNAs from HeLa cells was measured precisely by estimating the recovery rate of doped markers added before cell lysis (see Materials and Methods section). As shown in Table 1, the copy numbers of mRNAs ranged from 6000 (*ND5*) to 51 000 (*COX2*). The copy number of each mRNA was then plotted against its half-life (5) (Figure 1B). There is a clear correlation ($R^2 = 0.601$) between the copy number and half-life of each mRNA. Abundant mRNAs have a tendency toward longer half-lives, whereas less abundant mRNAs have shorter half-lives. These data strongly suggest that the steady-state levels of mRNAs in mitochondria are largely determined by their half-lives. Notable exceptions

Table 1. Copy numbers of human mitochondrial mRNAs in HeLa cells

mRNA	Copy numbers/cell	Half-life (min) (5)
ND1	38 000 ± 1600	74 ± 2
ND2	26 000 ± 1600	80 ± 6
COX1	37 000 ± 490	166 ± 29
COX2	51 000 ± 480	231 ± 18
ATP8/6	47 000 ± 1300	175 ± 13
COX3	34 000 ± 600	138 ± 10
ND3	15 000 ± 850	91 ± 4
ND4L/4	32 000 ± 1900	183 ± 5
ND5	6000 ± 73	77 ± 7
CYTB	16 000 ± 840	94 ± 24
ND6	14 000 ± 290	68 ± 10

are the mRNAs for *ND1* and *ND2*, which show relatively high abundance despite having shorter half-lives (74 and 80 min, respectively).

Mitochondrial mRNAs with longer half-lives are stabilized by the LRPPRC/SLIRP complex in HeLa cells

The LRPPRC/SLIRP complex has been assumed to play a regulatory role in post-transcriptional gene expression in human mitochondria (9). To clarify whether the LRPPRC/SLIRP complex is directly involved in the stabilization of mitochondrial mRNA, *SLIRP* mRNA was knocked down in HeLa cells. As shown in Figure 2A, mitochondrial transcription was specifically inhibited, and mRNA decay was observed. Upon knockdown of *SLIRP*, accelerated decay of *ND4L/4*, *COX1* and *CYTB* mRNAs was clearly observed, as compared to the control cells, while the decay of *ND3* mRNA was only modestly affected. This result provides direct evidence that SLIRP stabilizes mitochondrial mRNAs post-transcriptionally. Next, the steady-state level of each mRNA was measured after the knockdown of *LRPPRC* or *SLIRP* mRNA (Figure 2B and C). The mRNAs with longer half-lives tended to have a greater drop in their steady-state levels in the absence of SLIRP or LRPPRC than mRNAs with shorter half-lives. In addition, as previously mentioned (15), the patterns of relative change for each mRNA after either *LRPPRC* knockdown or *SLIRP* knockdown were markedly similar (Figure 2B and C, Supplementary Figure S1). This observation can be explained by the mutual stabilization of LRPPRC and SLIRP at the protein level (Figure 2D). After the knockdown of *SLIRP* mRNA, the endogenous levels of LRPPRC protein were also decreased. Similarly, knockdown of *LRPPRC* mRNA caused a specific reduction in endogenous SLIRP at the protein level. The mutual stabilization of these two proteins explains the finding that steady-state levels of SLIRP are significantly decreased in LSFC cells that express unstable LRPPRC with the A354V pathogenic point mutation (9). In addition, the patterns of the decreases in mRNA steady-state levels upon LRPPRC or SLIRP knockdown in HeLa cells (Figure 2B and C) were similar to those reported previously (15,16) in a human fibroblast cell line (MCH58). Thus, our observation is not confined to HeLa cells but is likely to be a general feature of mitochondrial mRNA metabolism in human cells.

The LRPPRC/SLIRP complex binds to mitochondrial mRNAs and their precursors

As both LRPPRC and SLIRP have RNA-binding domains (PPR and RRM, respectively), the LRPPRC/SLIRP complex was predicted to bind directly to RNAs in mitochondria. In fact, several mRNAs had been reported to coprecipitate with LRPPRC (9,17). However, whether the LRPPRC/SLIRP complex binds to other RNAs is unknown. To address this issue, HeLa cells were treated with formaldehyde to crosslink interacting RNAs and proteins, and endogenous LRPPRC was immunoprecipitated from the cell lysate. RNA recovery in the precipitant was analyzed by qRT-PCR (Figure 3A). All 11 mitochondrial mRNA species showed a high recovery ratio compared to cytoplasmic mRNAs and mitochondrial tRNAs, showing that the LRPPRC/SLIRP complex binds to all mRNA species in mitochondria. To elucidate whether the LRPPRC/SLIRP complex cotranscriptionally binds to precursor mRNAs, several sets of primers were designed to detect unprocessed bicistronic regions in precursor RNA: $tRNA^{Leu(UUR)}$-ND1 mRNA, $tRNA^{Met}$-ND2 mRNA, ATP8/6 mRNA-COX3 mRNA, $tRNA^{Phe}$-12 S rRNA and $tRNA^{Val}$-16 S rRNA. The three mRNA precursors were immunoprecipitated with the LRPPRC/SLIRP complex as efficiently as mature mRNAs (Figure 3A), while the two rRNA precursors were not (Figure 3A). These results showed that the LRPPRC/SLIRP complex was associated with the precursor mRNAs before processing, indicating that the LRPPRC/SLIRP binds to the mitochondrial transcripts cotranscriptionally.

The LRPPRC/SLIRP complex recognizes mRNA coding sequences

Most human mitochondrial mRNAs have little or no 5′ and 3′ untranslated regions (UTRs), and nine mRNAs (other than *ND5* and *ND6*) have poly(A) tails of ~50 nt in length (18). The LRPPRC/SLIRP complex can bind to the coding sequences and/or to the poly(A) tails of mRNAs. As we found that endogenous LRPPRC was coprecipitated with *ND5* and *ND6* mRNAs that have short and no poly(A) tails, respectively (4,18) (Figure 3A), the LRPPRC/SLIRP complex is not a poly(A)-specific RNA-binding protein. To characterize the mRNA-binding properties of the LRPPRC/SLIRP complex, the poly(A) tail length of *ND2* mRNA coprecipitated with LRPPRC-Flag was analyzed, because *ND2* mRNA has no 5′- or 3′-UTRs but has both poly(A) and oligoadenylated tails. If binding of the LRPPRC/SLIRP complex is poly(A)-specific, the population of mRNA that accumulated in the precipitant would only have poly(A) tails. However, no difference was observed in the population of mRNAs with poly(A) versus mRNAs with oligoadenylated tails (Figure 3B). To directly analyze the mRNA sequence that the LRPPRC/SLIRP complex binds to, RNA fragments of

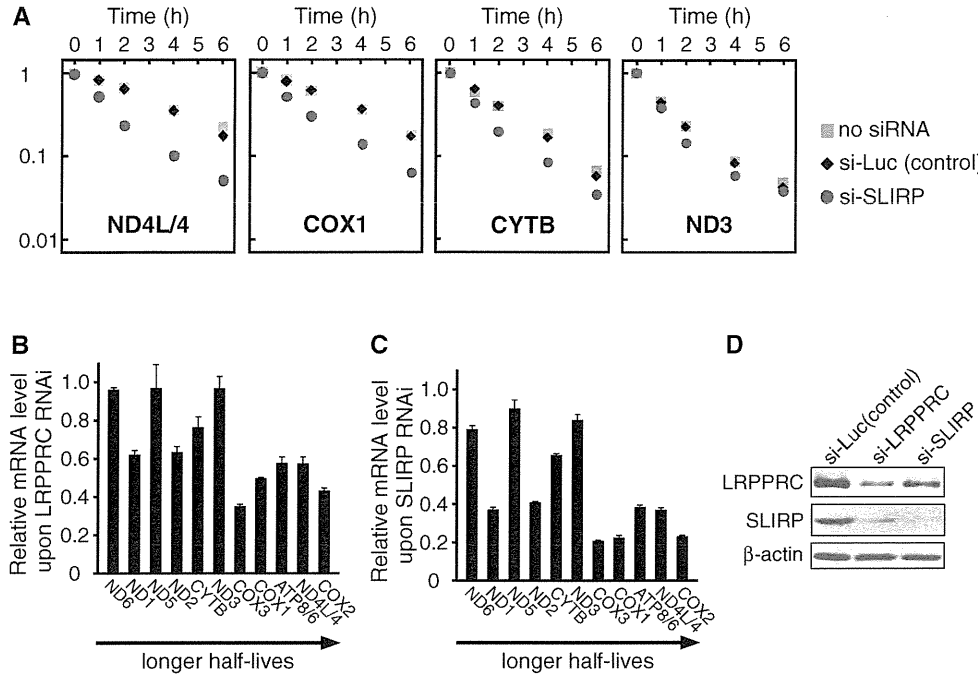

Figure 2. mRNAs with longer half-lives are stabilized by the LRPPRC/SLIRP complex. (**A**) Decay of *ND4L/4*, *COX1*, *CYTB* and *ND3* mRNAs in HeLa cells after siRNA-mediated knockdown of *SLIRP* (circles) or *luciferase* (diamonds) or without siRNA (squares). At 0, 1, 2, 4 or 6 h after the inhibition of mitochondrial transcription, total RNA was collected and each mRNA was quantified by qRT-PCR. All data were normalized to *GAPDH* mRNA. The vertical axis represents the relative mRNA level in logarithmic scale. The steady-state level of *SLIRP* mRNA decreased to 3% of that in the control cells upon siRNA-mediated knockdown. (**B** and **C**) Relative change in each mRNA level upon *LRPPRC* knockdown (B) or *SLIRP* knockdown (C) versus *luciferase* knockdown control cells, aligned in order of the mRNA's half-life (5). Mean values with SD were obtained from three independent experiments. The steady-state level of *LRPPRC* (B) and *SLIRP* (C) mRNAs dropped to 41% (B) and 1.2% (C), respectively, of those in the control cells. (**D**) Steady-state levels of endogenous LRPPRC and SLIRP after siRNA-mediated knockdown. Four days after siRNA transfection, endogenous LRPPRC and SLIRP in whole cell lysates were detected by western blotting.

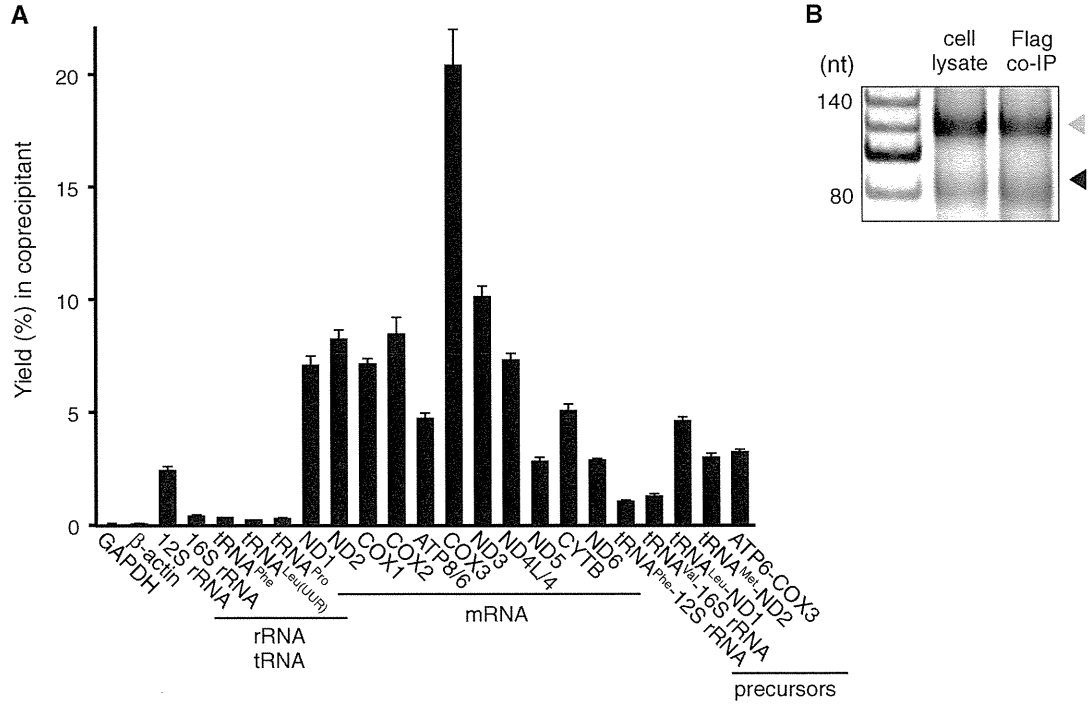

Figure 3. LRPPRC/SLIRP complex binds to mitochondrial mRNA coding sequences. (**A**) Yields of various RNAs and their precursors (%) co-immunoprecipitated with endogenous LRPPRC and quantified by qRT-PCR (means ± SD, $n = 3$). (**B**) A comparison of the poly(A) profiles of *ND2* mRNA in the cell lysate and in the precipitate obtained by pull-down of transiently expressed LRPPRC-Flag using the poly(A) tail length assay. The RT-PCR products derived from polyadenylated and oligoadenylated RNAs are indicated by the gray and black triangles, respectively. A 20-nt ladder is shown in the first lane.

mRNAs that coprecipitated with the LRPPRC/SLIRP complex from HeLa cells were cloned and sequenced (Supplementary Table S2). Of the 114 clones that were mapped to human transcripts, 112 clones were mapped to mtDNA, while 2 clones were from 28 S rRNA, confirming the quality of the immunoprecipitation. Of the 112 clones mapped to mtDNA, 97 clones mapped to the coding sequences of mitochondrial mRNAs. Notably, none of these 97 clones or other clones contained poly(A) or oligoadenylated tails at their 3′ ends. Therefore, it appears that the LRPPRC/SLIRP complex preferentially binds to the coding sequences of mitochondrial mRNAs and not to their poly(A) tails. In addition, one clone originating from the precursor mRNA containing $tRNA^{Leu(UUR)}$ and *ND1* was also obtained (Supplementary Table S2). This result supports our observation that the LRPPRC/SLIRP complex binds to precursor mRNAs (Figure 3A).

The LRPPRC/SLIRP complex is required to maintain poly(A) tails of mitochondrial mRNAs

mRNA metabolism in mitochondria was examined to gain mechanistic insight into mRNA stabilization mediated by the LRPPRC/SLIRP complex. Maintenance of the poly(A) tail is required for the stability of several mRNAs, including *COX1*, *COX2*, *COX3* and *ATP8/6* (5,19). Therefore, changes in the poly(A) tail length of several mRNAs were measured when the LRPPRC/SLIRP complex was inactivated by RNAi. Under control conditions (si-Luc), both poly- and oligoadenylated mRNAs were observed (Figure 4A). When MTPAP was knocked down as a positive control experiment, a decrease in the number of polyadenylated mRNAs and the accumulation of no (or oligo-) adenylated mRNAs was observed (Figure 4A). After the knockdown of LRPPRC or SLIRP, oligoadenylated mRNAs of *COX1*, *COX3* and *CYTB* clearly accumulated, in conjunction with a reduction in the population of polyadenylated mRNAs (Figure 4A). For *ND2* and *ND3*, a slight increase in oligoadenylated mRNAs was observed, but the effect was limited. As *ND5* mRNA has a short poly(A) tail (18), little change in the mRNA profile occurred after the knockdown of LRPPRC or SLIRP (Figure 4A). These results indicate that the LRPPRC/SLIRP complex is required for the maintenance of polyadenylated mRNAs. It should be noted that mRNAs (*COX1* and *COX3*) that are strongly stabilized by the LRPPRC/SLIRP complex tend to have a larger poly(A)/oligo(A) ratio. This suggests that the LRPPRC/SLIRP complex might stabilize mRNAs by suppressing 3′deadenylation and/or 3′exonucleolytic degradation.

PNPase and SUV3 are involved in mRNA degradation in human mitochondria

In human mitochondria, mRNA turnover associated with 3′ terminal metabolism has been extensively studied (23). However, the major component of the RNA degradation machinery has yet to be identified. Our group previously reported that PNPase is involved in 3′ deadenylation of several mRNAs (19). In addition, recombinant PNPase and SUV3 helicase cooperatively degrade RNA *in vitro* (30). However, whether PNPase is a *bona fide* 3′ exonuclease in mitochondria has been a controversial issue (23), because PNPase has multivalent functions, including the RNA import of RNase MRP RNA into the mitochondria (26) and the degradation of cytoplasmic mRNA (27) and miRNAs (28). Recently, 2′-phosphodiesterase (PDE12) was found to localize to mitochondria and to possess 3′–5′ exonucleolytic activity for RNAs *in vitro*, and *PDE12* overexpression promoted deadenylation in cultured cells (22,38).

To identify the primary component of the RNA degradation machinery, *PNPase* or *PDE12* was knocked down by RNAi, mitochondrial transcription was specifically inhibited and mRNA decay was monitored (Figure 4B). In control cells, the level of each mRNA decreased in accordance with its specific half-life. Upon knockdown of *PNPase*, mRNA decay almost completely halted (Figure 4B). On the other hand, when *PDE12* was knocked down, the steady-state levels of mRNAs (*COX1*, *CYTB*, *ATP8/6* and *ND5*) increased slightly (~1.3-fold; Supplementary Figure S2), as previously reported (38). However, the rate of mRNA decay was only slightly affected by the inactivation of *PDE12* (Figure 4B). These results, together with previous studies (19,30), clearly demonstrate that PNPase is the primary 3′–5′ exonuclease responsible for the degradation of mRNAs in human mitochondria. In addition, PNPase functions not only as a deadenylase but also as an exonuclease, because the inactivation of *PNPase* also inhibited the degradation of *ND5* mRNA (Figure 4B), which is rarely polyadenylated (18).

The recombinant form of the human homolog of yeast Suv3p (SUV3) forms a complex with PNPase, which degrades RNA in the 3′–5′ direction *in vitro* (30), and SUV3 is involved in mitochondrial mRNA degradation in the cell (31). To investigate whether SUV3 helicase is absolutely necessary for the degradation of mitochondrial mRNAs, mRNA decay was monitored after knockdown of *SUV3* expression. Similar to the effect of the knockdown of *PNPase*, the decay of each mRNA was halted (Figure 4B). Therefore, both SUV3 helicase and PNPase are essential for mRNA degradation in human mitochondria.

Taken together with the accelerated decay of several mRNAs upon *SLIRP* knock down (Figure 2A), the results suggest that the LRPPRC/SLIRP complex stabilizes a set of mRNAs by suppressing 3′–5′ exonuclease activity performed by PNPase and SUV3.

LRPPRC promotes MTPAP-mediated polyadenylation of mRNAs

Next, we examined whether the LRPPRC/SLIRP complex has a function to promote polyadenylation of mRNAs. In six species of mRNAs (Figure 5A), oligoadenylated forms clearly accumulated when SLIRP was inactivated (as observed in Figure 4A), and elongated poly(A) tails were observed upon knockdown of PNPase, as previously reported (19). Upon the simultaneous knockdown of *SLIRP* and *PNPase* (Figure 5A), the oligoadenylated

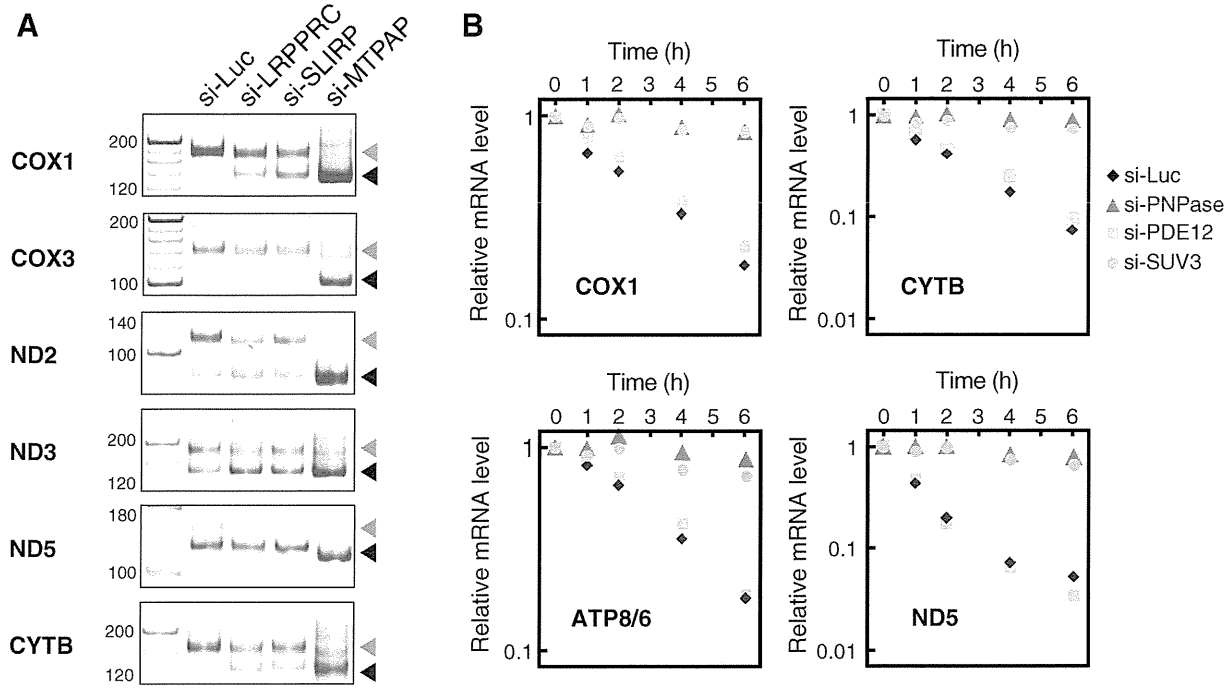

Figure 4. PNPase and SUV3 are primarily involved in degradation of human mitochondrial mRNAs. (**A**) Polyadenylation profile of mitochondrial mRNAs upon *LRPPRC* or *SLIRP* knockdown. The 3′ termini of the mRNAs for *COX1*, *COX3*, *ND2*, *ND3*, *ND5* and *CYTB* in HeLa cells transfected with siRNAs for *luciferase*, *LRPPRC*, *SLIRP* or *MTPAP* were analyzed by the poly(A) tail length assay. RT-PCR products derived from polyadenylated and oligoadenylated RNAs are indicated by gray and black triangles, respectively. The first lanes show the 20-nt ladders. (**B**) Decay of *COX1*, *CYTB*, *ATP8/6* and *ND5* mRNAs in HeLa cells after knockdown with siRNA against *luciferase* (diamonds), *PDE12* (squares), *PNPase* (triangles) or *SUV3 helicase* (circles). At 0, 1, 2, 4 or 6 h after the inhibition of mitochondrial transcription, total RNA was collected and each mRNA was quantified by qRT-PCR. All data were normalized to *GAPDH* mRNA. The vertical axis represents the relative mRNA level in logarithmic scale. The steady-state level of *PNPase*, *SUV3* and *PDE12* mRNAs dropped to 11.1%, 11.9% and 22%, respectively, of those in the control cells.

forms of *COX1*, *COX2*, *ND3* and *CYTB* mRNAs accumulated to slightly higher levels than those observed after single knockdown of PNPase, suggesting that the LRPPRC/SLIRP complex promotes the polyadenylation of some mRNAs. Although we cannot rule out completely the possibility that insufficient PNPase knockdown led to the persistence of weak deadenylation activity under these conditions, we speculate that mitochondrial poly(A) polymerase (MTPAP) cannot efficiently synthesize poly(A) tails of mRNAs in the absence of the LRPPRC/SLIRP complex.

To demonstrate whether the LRPPRC/SLIRP complex plays a functional role in promoting polyadenylation of mRNAs, we conducted an *in vitro* polyadenylation experiment using recombinant proteins. Either *COX2* or *COX3* mRNA transcript was oligoadenylated with the recombinant MTPAP in the presence of [α-^{32}P] ATP (Figure 5B). Polyadenylation of these mRNAs was stimulated in a dose-dependent manner after the addition of recombinant LRPPRC (Figure 5B), indicating that LRPPRC directly promoted MTPAP-mediated polyadenylation of mRNAs *in vitro*. Only a small effect of recombinant SLIRP on polyadenylation was observed (data not shown), indicating that LRPPRC plays the dominant role in promoting polyadenylation, while SLIRP plays a supportive role in stabilizing LRPPRC in the cell (Figure 2D).

To gain mechanistic insights into the functional role of LRPPRC in MTPAP-mediated polyadenylation, we characterized the substrate specificity of MTPAP. Considering that LRPPRC has PPR motifs that bind to single-stranded RNAs (11,13), we speculated that the LRPPRC/SLIRP complex binds to mRNAs and prevents their 3′-terminal regions forming secondary/tertiary structures, facilitating the polyadenylation by MTPAP. In fact, a plant PPR motif protein (PPR10) was shown to unwind a hairpin RNA structure and recognize a single-stranded target sequence (39). This observation inspired us to examine whether MTPAP preferentially adenylates the single-stranded termini of mRNAs. As a model substrate, we used a 62-nt-long single-stranded (ss)RNA (with an mfold prediction folding $\Delta G = -1.4\,\mathrm{kcal \cdot mol^{-1}}$), corresponding to the 3′ terminal region of *ND1* mRNA (Figure 5C). This ssRNA was oligoadenylated efficiently and was polyadenylated to some extent (Figure 5C). When the ssRNA was hybridized with complementary RNAs to prepare double-stranded (ds)RNA substrates with 0- and 3-nt 3′ overhangs, the dsRNAs were hardly adenylated (Figure 5C). In contrast, the dsRNA with a 10-nt 3′ overhang was adenylated by MTPAP (Figure 5C). These results clearly demonstrate that MTPAP specifically adenylates RNAs with a single-stranded 3′-end. *ND5* and *ND6* mRNAs

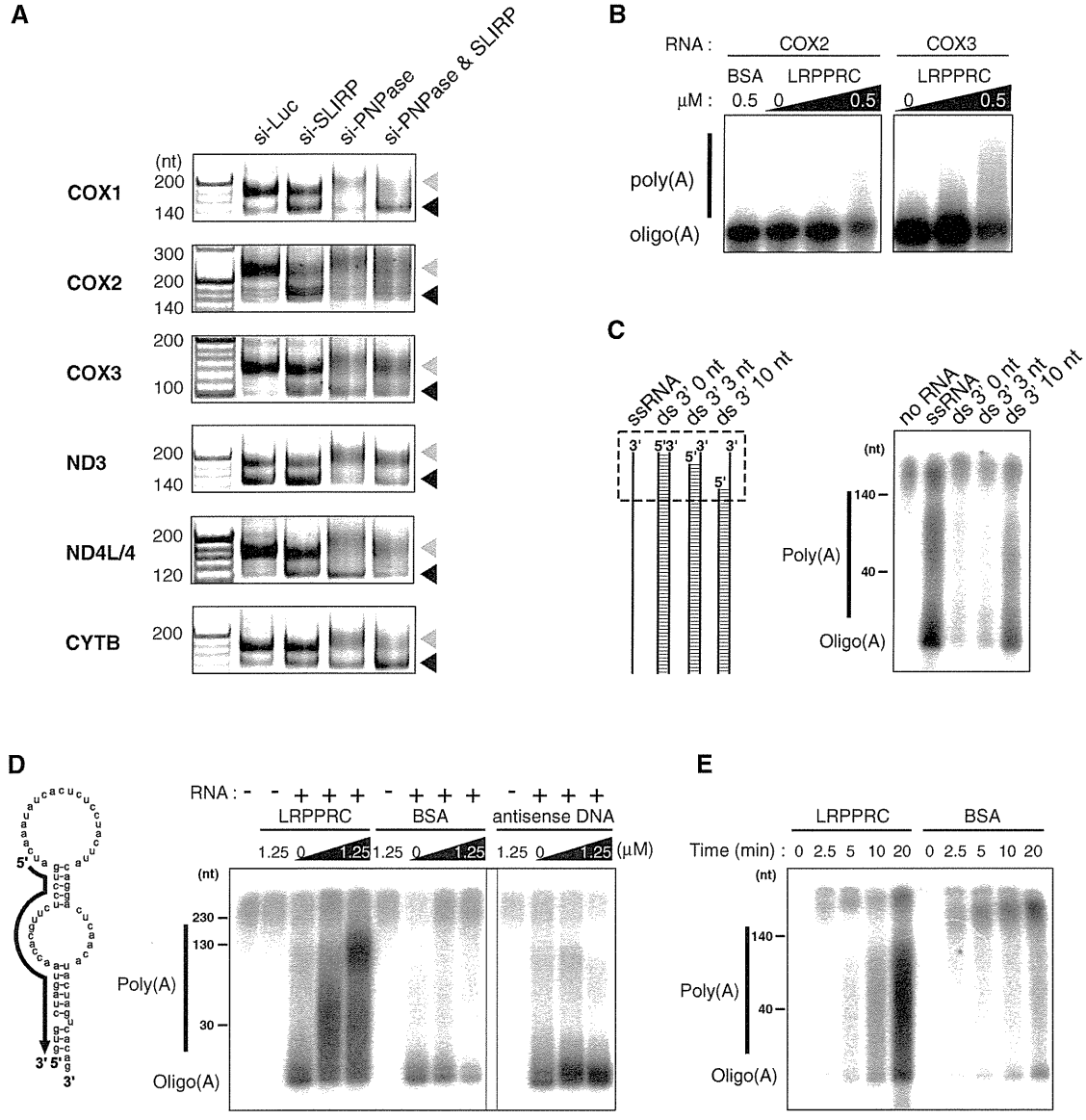

Figure 5. LRPPRC promotes MTPAP-mediated polyadenylation of mRNAs. (**A**) Polyadenylation profile of mitochondrial mRNAs upon knockdown of *luciferase*, *SLIRP* and *PNPase* or double knockdown of *SLIRP* and *PNPase*. The 3′ termini of the mRNAs for *COX1*, *COX2*, *COX3*, *ND3*, *ND4L/4* and *CYTB* in HeLa cells transfected with siRNAs were analyzed by the poly(A) tail length assay. RT-PCR products derived from polyadenylated and oligoadenylated RNAs are indicated by gray and black triangles, respectively. The first lanes show 20-nt ladders. (**B**) *In vitro* polyadenylation of *COX2* or *COX3* mRNA transcript catalyzed by recombinant MTPAP in the presence of [α-^{32}P] ATP and different amounts of recombinant LRPPRC (0, 0.1 or 0.5 μM) or BSA (0.5 μM). The products were resolved by polyacrylamide gel electrophoresis and the radioactivity was visualized by using an imaging analyzer (B–E). (**C**) *In vitro* polyadenylation of single-stranded (ss) or double-stranded (ds) RNA substrates, catalyzed by recombinant MTPAP in the presence of [α-^{32}P] ATP. Schematic depiction of the substrates is shown on the left. The regions containing 3′ ss overhang of each substrate are boxed in the dotted line. (**D**) *In vitro* polyadenylation of the structured RNA (shown on the left) catalyzed by recombinant MTPAP in the presence of [α-^{32}P] ATP and different amounts of recombinant LRPPRC (0, 0.25 or 1.25 μM), BSA (0, 0.25 or 1.25 μM) or antisense DNA (0, 0.25 or 1.25 μM). The complementary region of the antisense oligo, shown as a solid arrow, is depicted on the structured RNA substrate. (**E**) The time course representation of the *in vitro* polyadenylation of the ssRNA in the presence of LRPPRC or BSA. 1.25 μM of each protein was added to the reaction mixture.

have short and no poly(A) tails, respectively (4,18). In addition, *ND5* and *ND6* mRNAs are the only mitochondrial mRNAs with long 3′ UTRs (4,18). The 3′ UTR of *ND5* is complementary to the *ND6* coding sequence; conversely, the *ND6* 3′ UTR is complementary to the *ND5* coding sequence (Figure 1A). Some fractions of *ND5* and *ND6* mRNAs can hybridize with each other to form a duplex structure. This would prevent MTPAP from performing polyadenylatation, because MTPAP preferentially polyadenylates RNAs with single-stranded 3′ ends (Figure 5C). In addition, deep sequence analysis detected abundant antisense transcripts that were complementary to *ND5* and *ND6* mRNAs in human mitochondria (40). These transcripts might be involved in the suppression of polyadenylation. Alternatively, 3′ UTRs of *ND5* and *ND6* mRNAs may form stable

intramolecular tertiary structures that prevent polyadenylation by MTPAP.

Mitochondrial mRNAs, in general, form complex secondary structures (41), which might prevent polyadenylation by MTPAP. We next designed a structured RNA substrate with a duplex 3′-end (mfold folding $\Delta G = -12.8\,\text{kcal}\cdot\text{mol}^{-1}$) (Figure 5D) that mimics the 3′ terminal region of mitochondrial mRNAs. When the substrate was used for *in vitro* polyadenylation in the absence of LRPPRC, a small portion of this transcript was oligoadenylated (Figure 5D), whereas in the presence of LRPPRC, polyadenylation occurred in a dose-dependent manner (Figure 5D). A poly(A) tail of up to about 150 nt was observed under this condition. Addition of BSA instead of LRPPRC did not show any effect on polyadenylation (Figure 5D), showing that the increased poly(A) synthesis by LRPPRC is not caused by non-specific stabilization of MTPAP by increased protein concentration. Next, we replaced LRPPRC with a DNA probe that is complementary to the 5′ half of the substrate used for *in vitro* polyadenylation. The DNA probe hybridizes to the structured RNA substrate, liberating its 3′-end as a single strand. Surprisingly, addition of the DNA probe only resulted in the accumulation of oligoadenylated RNA (Figure 5D) with no clear enhancement of polyadenylation (Figure 5D). In addition, when the ssRNA was employed as a substrate for *in vitro* polyadenylation, efficient polyadenylation was observed in the presence of LRPPRC (Figure 5E). These data demonstrated that the single-stranded 3′-end of RNA is not sufficient for polyadenylation and that MTPAP requires LRPPRC for efficient elongation of polyadenylated chains.

DISCUSSION

In this report, we describe the first absolute quantification of mitochondrial mRNAs in a human cell. The copy numbers of mitochondrial mRNAs ranged from 6000 (*ND5*) to 51 000 (*COX2*) per cell. Thus, an up to 8.5-fold difference in the steady-state levels of mRNAs from the long H-strand transcript was observed. We also noted good correlation between the copy number and the half-life of each mRNA ($R^2 = 0.601$). Abundant mRNAs, such as *COX1*, *COX2*, *COX3*, *ATP8/6* and *ND4L/4*, have longer half-lives, whereas less abundant mRNAs, such as *ND3*, *ND5* and *CYTB*, have shorter half-lives. These data indicate that the steady-state levels of mitochondrial mRNAs in human HeLa cells are basically determined by their half-lives. Notable exceptions are *ND1* and *ND2* mRNAs, which were relatively abundant despite having short half-lives (74 and 80 min, respectively). According to the gene organization of mtDNA (Figure 1A), *ND1* and *ND2* are localized at the beginning of the long H-strand transcript. Recently, it was reported that TEFM (transcription elongation factor of mitochondria), which is a partner protein of mitochondrial RNA polymerase (POLRMT), is required for synthesizing promoter-distal transcripts from both strands (42). Limited availability of TEFM in rapidly growing cells might result in an increase of promoter-proximal transcripts. Alternatively, as mtDNAs are damaged by reactive oxygen species and aldehydes, H-strand transcription by POLRMT might be arrested by damaged bases in mtDNA (43), which produces shorter H-strand transcripts.

PPR motif-containing proteins constitute a large family of RNA-binding proteins that are primarily found in higher plants (44,45). In general, most proteins bearing PPR motifs bind to specific RNA sequences (44). This sequence-specific recognition is accomplished by the alignment of PPR motifs. Although LRPPRC contains 16 PPR motifs (12), the LRPPRC/SLIRP complex does not show strong sequence specificity for mRNA binding. In fact, all mRNA species were coprecipitated with the LRPPRC/SLIRP complex (Figure 3A). Sequence analysis of the bound RNA fragments revealed that the LRPPRC/SLIRP complex bound to mRNA coding regions and not to poly(A) tails (Supplementary Table S2). This result is in good agreement with an *in vitro* study that showed LRPPRC does not bind to poly(A) RNA immobilized on beads (11). In addition, *ND5* and *ND6* mRNAs, which have little or no poly(A) tails, were also coprecipitated with the LRPPRC/SLIRP complex (Figure 3A). Collectively, these data showed that the LRPPRC/SLIRP complex directly binds to mRNA coding sequences without strong sequence specificity. Nonetheless, considering the different degrees of mRNA stabilization by the LRPPRC/SLIRP complex (Figure 2B and C), there might still exist some specific sequences in these mRNAs that are preferentially recognized by the LRPPRC/SLIRP complex.

The ND6 mRNA is only weakly coprecipitated with LRPPRC-Flag in the absence of crosslinking (17). We performed immunoprecipitation of the RNP complex with endogenous LRPPRC from the cells that were crosslinked with formaldehyde (Figure 3A). The data showed that ND6 mRNA was coprecipitated with LRPPRC, when compared to control tRNAs and cytoplasmic RNAs, but the efficiency of coprecipitation was relatively low (Figure 3A). This indicates that the LRPPRC/SLIRP complex is weakly associated with ND6 mRNAs in mitochondria. In addition to mitochondrial mRNAs, a small amount of 12 S rRNA was observed in the LRPPRC immunoprecipitate (Figure 3A). The 28S small subunit of mammalian mitochondrial ribosome binds to mitochondrial mRNA even in the absence of auxiliary factors, whereas the large subunit does not (46). Thus, under crosslinking conditions, the 12 S rRNA in the 28 S subunit might have been coprecipitated with the LRPPRC/SLIRP complex through its tethering to mRNAs.

According to proteomic data (47), LRPPRC and SLIRP are abundant in mitochondria. We roughly estimated the copy numbers of LRPPRC in HeLa cells by western blotting, using recombinant LRPPRC as a reference (see 'Materials and Methods' section), and found approximately 2.0×10^6 LRPPRC molecules per cell. Given that there are 316 000 mitochondrial mRNA molecules in each HeLa cell (Table 1), the average number of LRPPRC to each mRNA would be 6, or 1 LRPPRC

per 170 nt of mitochondrial mRNA. Such a high abundance of LRPPRC in mitochondria may facilitate cotranscriptional binding of the LRPPRC/SLIRP complex to many locations on the mRNA coding sequence, which could potentially affect mRNA secondary/tertiary structure.

How does the LRPPRC/SLIRP complex specifically discriminate mRNA regions from tRNAs and rRNAs in the precursor RNA? As the LRPPRC/SLIRP complex binds to mRNA coding regions without much sequence specificity, once transcription begins, the LRPPRC/SLIRP complex is loaded onto the nascent chain (Figure 6). By contrast, tRNAs spontaneously fold into secondary and tertiary structures that are recognized by various RNA-modifying enzymes and processing endonucleases, including RNaseP (*MRPP1,2,3*) (48) and tRNase Z (*ELAC2*) (49), which separate tRNAs, mRNAs and rRNAs from polycistronic transcripts. During this process, the LRPPRC/SLIRP complex would probably be unable to access tRNA regions, because PPR motifs generally bind to single-stranded RNAs (13). Moreover, the precursor RNAs, including both 12S and 16S rRNAs, also fold into programmed secondary and tertiary structures, which result in the recruitment of dozens of ribosomal proteins and non-ribosomal factors for their assembly into small and large ribosomal particles. Little is known about the mitoribosome assembly mechanism. However, as the assembly of bacterial ribosomes takes place cotranscriptionally (50), mitochondrial rRNAs and ribosomal proteins are also likely to assemble cotranscriptionally; thus, the ribosomal proteins are likely to bind to rRNAs with more specificity and affinity than the LRPPRC/SLIRP complex. This speculation would explain our observation that the LRPPRC/SLIRP complex was not efficiently coprecipitated with the precursor transcripts composed of tRNA and rRNA (Figure 3A). Therefore, the mRNA specificity of the LRPPRC/SLIRP complex might be established by a passive mechanism in which tRNA and rRNA regions are excluded from binding to the LRPPRC/SLIRP complex.

We have shown that PNPase and SUV3 are essential factors for mRNA degradation in human mitochondria. As knockdown of either *PNPase* or *SUV3* alone inhibited mitochondrial mRNA decay (Figure 4B), PNPase and SUV3 helicase are likely to cooperatively degrade mitochondrial mRNAs in the cell. This speculation was also supported by the fact that recombinant PNPase and SUV3 form a heteropentamer which degrades dsRNA *in vitro* (30). However, in HeLa cell lines in which *PNPase* was stably silenced by RNAi (51), *ND3* and *ND5* poly(A) tails were elongated, while the *COX3* poly(A) tail was unaffected and *COX1* lost its poly(A) tail, indicating that PNPase is indirectly involved in poly(A) metabolism. This result conflicts with our observation that transient knockdown of *PNPase* caused poly(A) elongation in most of transcripts, including *COX1* and *COX3* (Figure 5) (19). In fact, in their article (51), transient *PNPase* silencing was shown to cause elongation of the *COX1* mRNA poly(A) tail, which was clearly self-contradictory. PNPase has multivalent functions, including the transport of the RNA component for RNaseMRP into mitochondria (26) and the degradation of cytoplasmic mRNA (27) and miRNA (28). Thus, long-term, stable *PNPase* silencing (51) may have caused various secondary effects. Also, some revertants to complement the reduced PNPase function might have arisen.

Although we have strong evidence that PNPase is directly involved in deadenylation and degradation of mRNAs in human mitochondria, the steady-state levels of several mRNAs and proteins were unchanged upon knockdown of *PNPase* (19,25). If PNPase functions only in mRNA degradation, downregulation of *PNPase* should

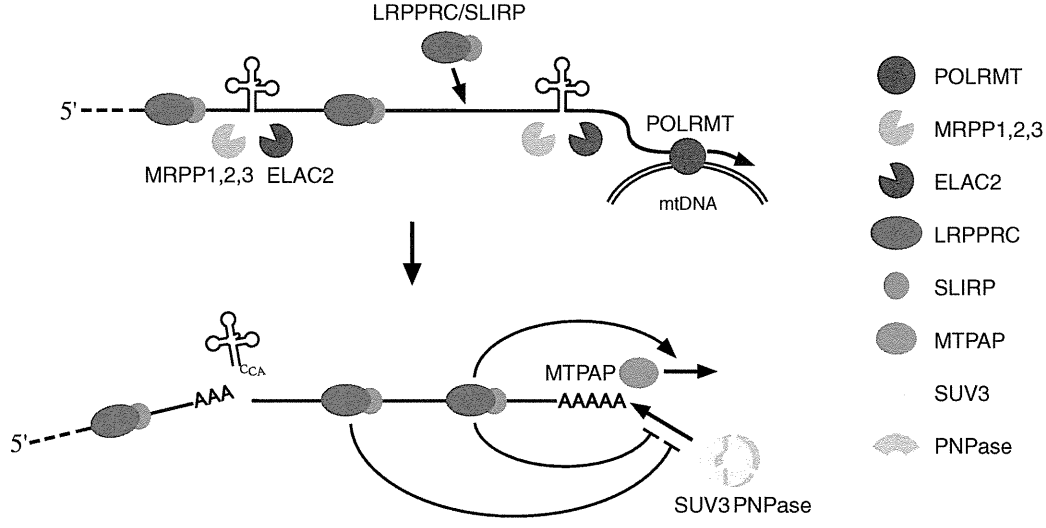

Figure 6. Schematic depiction of biogenesis and the metabolism of mRNAs in human mitochondria. As mitochondrial RNA polymerase (POLRMT) transcribes mtDNA, the LRPPRC/SLIRP complex binds to the mRNA coding sequences of the long polycistronic precursor. tRNA 5′ and 3′ processing conducted by MRPP1,2,3 (48) and ELAC2 (49) generate mRNAs that are bound to the LRPPRC/SLIRP complex. The LRPPRC/SLIRP complex promotes mRNA polyadenylation by MTPAP. The LRPPRC/SLIRP complex protects mRNAs from 3′ exonucleolytic degradation mediated by PNPase and SUV3 helicase.

have resulted in the accumulation of mitochondrial mRNAs and proteins to some extent. PNPase is also involved in the mitochondrial import of the RNA component for RNaseMRP (26), which is an essential factor for generating the RNA primers required for the initiation of mtDNA replication (52). This fact prompted us to speculate that PNPase might be involved in the maintenance of mtDNA steady-state level. To investigate this possibility, we quantified the mtDNA level when *PNPase* was knocked down. As expected, *PNPase* knockdown caused a decrease in the mtDNA level (Supplementary Figure S3A), which could have decreased the transcriptional level of mRNAs, thereby counteracting the accumulation of mitochondrial mRNAs caused by loss of *PNPase* exonucleolytic activity. Four days after *PNPase* knockdown, the mtDNA level was 15% of the control level. However, mRNA degradation had almost completely stopped at this time (Figure 4B). When *PNPase* was knocked down for 2 days and the mtDNA level decreased to about 50% (Supplementary Figure S3A), a clear halt in mRNA degradation was still observed (Supplementary Figure S3B). As the measurement of mRNA degradation is independent of changes in mtDNA copy number, the results in this study cannot be easily attributed to a secondary effect of a decrease in the mtDNA level upon *PNPase* knockdown.

The LRPPRC/SLIRP complex was found to stabilize mRNAs by suppressing 3′ exonucleolytic degradation catalyzed by PNPase and SUV3. The mechanism by which the LRPPRC/SLIRP complex suppresses mRNA degradation awaits further elucidation. As the LRPPRC/SLIRP complex bound to mRNA coding sequences and not to poly(A) tails (Figure 3B and Supplementary Table S2), the LRPPRC/SLIRP complex could not directly impede deadenylation by PNPase and SUV3 by covering the poly(A) tail. Considering that PNPase and SUV3 preferentially degrade dsRNAs with a 3′ overhang (30), we speculate that the binding of the LRPPRC/SLIRP complex to the coding regions of mRNAs inhibits the folding of their 3′ termini into secondary/tertiary structures, thereby preventing mRNAs from becoming good substrates for degradation. Otherwise, if the poly(A) tail hybridizes with the uridine-rich region in the coding sequence to form intramolecular dsRNA, the LRPPRC/SLIRP complex might be involved in releasing the poly(A) tail from the coding region, which would make it a poor substrate for 3′exonucleolytic degradation by PNPase and SUV3.

A loss of poly(A) tails was found in mitochondrial mRNAs from a *LRPPRC* null mouse (17). Similarly, loss of poly(A) tails and accumulation of oligo(A) tails were observed in mitochondrial mRNAs from the RNAi knockdown flies of bicoid stability factor, which is a homolog of *LRPPRC* in *Drosophila* (53). These reports demonstrated that the LRPPRC/SLIRP complex is necessary to maintain mitochondrial mRNA poly(A) tails. In accordance with these reports, knockdown of *LRPPRC* or *SLIRP* in HeLa cells caused the accumulation of oligoadenylated mRNAs with a reduced population of polyadenylated mRNAs (Figure 4A). We have shown that the LRPPRC/SLIRP complex promotes mRNA poly(A) synthesis (Figure 5A and B). More precisely, the LRPPRC/SLIRP complex is likely to be involved in the unwinding the 3′ terminus in the initiation step of adenylation (oligoadenylation), because MTPAP preferentially adenylates RNA substrates bearing a single-stranded 3′ terminus (Figure 5C). In fact, artificial unwinding of the structured RNA substrate by the antisense DNA enhanced its oligoadenylation by MTPAP (Figure 5D). The most important finding in this experiment was that LRPPRC also promoted the elongation step of polyadenylation (Figure 5D and E). Further studies will be necessary to reveal how LRPPRC promotes poly(A) elongation. Our observation would explain why the mitochondrial mRNA poly(A) tail was lost and the oligo(A) tail was retained in a *LRPPRC* null mouse (17).

In conclusion, we report the different steady-state levels of human mitochondrial mRNAs through the accurate determination of their copy numbers. We also show a clear correlation between copy number and the half-life of each mRNA. mRNAs with longer half-lives are stabilized by the LRPPRC/SLIRP complex, which cotranscriptionally binds to mRNA coding sequences, promotes mRNA poly(A) elongation and suppresses 3′exonucleolytic degradation mediated by PNPase and SUV3.

SUPPLEMENTARY DATA

Supplementary Data is available at NAR Online: Supplementary Figures 1–3 and Supplementary Tables 1 and 2.

ACKNOWLEDGEMENTS

We are grateful to the members of the Suzuki laboratory for fruitful discussions and suggestions. We also thank Drs. Masayuki Sakurai (University of Pennsylvania), Shinichi Nakagawa (RIKEN) and Yuko Hasegawa (RIKEN) for technical support.

FUNDING

Grants-in-Aid for Scientific Research on Priority Areas from the Ministry of Education, Science, Sports and Culture of Japan (to T.S.); New Energy and Industrial Technology Development Organization (NEDO) (to T.S.). Funding for open access charge: Japan Ministry of Education, Science, Sports and Culture.

Conflict of interest statement. None declared.

REFERENCES

1. Anderson,S., Bankier,A.T., Barrell,B.G., de Bruijn,M.H., Coulson,A.R., Drouin,J., Eperon,I.C., Nierlich,D.P., Roe,B.A., Sanger,F. *et al.* (1981) Sequence and organization of the human mitochondrial genome. *Nature*, **290**, 457–465.
2. Ojala,D., Montoya,J. and Attardi,G. (1981) tRNA punctuation model of RNA processing in human mitochondria. *Nature*, **290**, 470–474.

3. Duborjal,H., Beugnot,R., Mousson de Camaret,B. and Issartel,J.P. (2002) Large functional range of steady-state levels of nuclear and mitochondrial transcripts coding for the subunits of the human mitochondrial OXPHOS system. *Genome Res.*, **12**, 1901–1909.
4. Slomovic,S., Laufer,D., Geiger,D. and Schuster,G. (2005) Polyadenylation and degradation of human mitochondrial RNA: the prokaryotic past leaves its mark. *Mol. Cell. Biol.*, **25**, 6427–6435.
5. Nagao,A., Hino-Shigi,N. and Suzuki,T. (2008) Measuring mRNA decay in human mitochondria. *Methods Enzymol.*, **447**, 489–499.
6. Morin,C., Mitchell,G., Larochelle,J., Lambert,M., Ogier,H., Robinson,B.H. and De Braekeleer,M. (1993) Clinical, metabolic, and genetic aspects of cytochrome C oxidase deficiency in Saguenay-Lac-Saint-Jean. *Am. J. Hum. Genet.*, **53**, 488–496.
7. Merante,F., Petrova-Benedict,R., MacKay,N., Mitchell,G., Lambert,M., Morin,C., De Braekeleer,M., Laframboise,R., Gagne,R. and Robinson,B.H. (1993) A biochemically distinct form of cytochrome oxidase (COX) deficiency in the Saguenay-Lac-Saint-Jean region of Quebec. *Am. J. Hum. Genet.*, **53**, 481–487.
8. Mootha,V.K., Lepage,P., Miller,K., Bunkenborg,J., Reich,M., Hjerrild,M., Delmonte,T., Villeneuve,A., Sladek,R., Xu,F. *et al.* (2003) Identification of a gene causing human cytochrome c oxidase deficiency by integrative genomics. *Proc. Natl Acad. Sci. USA*, **100**, 605–610.
9. Sasarman,F., Brunel-Guitton,C., Antonicka,H., Wai,T. and Shoubridge,E.A. (2010) LRPPRC and SLIRP interact in a ribonucleoprotein complex that regulates posttranscriptional gene expression in mitochondria. *Mol. Biol. Cell*, **21**, 1315–1323.
10. Xu,F., Morin,C., Mitchell,G., Ackerley,C. and Robinson,B.H. (2004) The role of the LRPPRC (leucine-rich pentatricopeptide repeat cassette) gene in cytochrome oxidase assembly: mutation causes lowered levels of COX (cytochrome c oxidase) I and COX III mRNA. *Biochem. J.*, **382**, 331–336.
11. Mili,S. and Pinol-Roma,S. (2003) LRP130, a pentatricopeptide motif protein with a noncanonical RNA-binding domain, is bound in vivo to mitochondrial and nuclear RNAs. *Mol. Cell. Biol.*, **23**, 4972–4982.
12. Sterky,F.H., Ruzzenente,B., Gustafsson,C.M., Samuelsson,T. and Larsson,N.G. (2010) LRPPRC is a mitochondrial matrix protein that is conserved in metazoans. *Biochem. Biophys. Res. Commun.*, **398**, 759–764.
13. Small,I.D. and Peeters,N. (2000) The PPR motif—a TPR-related motif prevalent in plant organellar proteins. *Trends Biochem. Sci.*, **25**, 46–47.
14. Hatchell,E.C., Colley,S.M., Beveridge,D.J., Epis,M.R., Stuart,L.M., Giles,K.M., Redfern,A.D., Miles,L.E., Barker,A., MacDonald,L.M. *et al.* (2006) SLIRP, a small SRA binding protein, is a nuclear receptor corepressor. *Mol. Cell*, **22**, 657–668.
15. Gohil,V.M., Nilsson,R., Belcher-Timme,C.A., Luo,B., Root,D.E. and Mootha,V.K. (2010) Mitochondrial and nuclear genomic responses to loss of LRPPRC expression. *J. Biol. Chem.*, **285**, 13742–13747.
16. Baughman,J.M., Nilsson,R., Gohil,V.M., Arlow,D.H., Gauhar,Z. and Mootha,V.K. (2009) A computational screen for regulators of oxidative phosphorylation implicates SLIRP in mitochondrial RNA homeostasis. *PLoS Genet.*, **5**, e1000590.
17. Ruzzenente,B., Metodiev,M.D., Wredenberg,A., Bratic,A., Park,C.B., Camara,Y., Milenkovic,D., Zickermann,V., Wibom,R., Hultenby,K. *et al.* (2012) LRPPRC is necessary for polyadenylation and coordination of translation of mitochondrial mRNAs. *EMBO J.*, **31**, 443–456.
18. Temperley,R.J., Wydro,M., Lightowlers,R.N. and Chrzanowska-Lightowlers,Z.M. (2010) Human mitochondrial mRNAs—like members of all families, similar but different. *Biochim. Biophys. Acta*, **1797**, 1081–1085.
19. Nagaike,T., Suzuki,T., Katoh,T. and Ueda,T. (2005) Human mitochondrial mRNAs are stabilized with polyadenylation regulated by mitochondria-specific poly(A) polymerase and polynucleotide phosphorylase. *J. Biol. Chem.*, **280**, 19721–19727.
20. Tomecki,R., Dmochowska,A., Gewartowski,K., Dziembowski,A. and Stepien,P.P. (2004) Identification of a novel human nuclear-encoded mitochondrial poly(A) polymerase. *Nucleic Acids Res.*, **32**, 6001–6014.
21. Wydro,M., Bobrowicz,A., Temperley,R.J., Lightowlers,R.N. and Chrzanowska-Lightowlers,Z.M. (2010) Targeting of the cytosolic poly(A) binding protein PABPC1 to mitochondria causes mitochondrial translation inhibition. *Nucleic Acids Res.*, **38**, 3732–3742.
22. Rorbach,J., Nicholls,T.J. and Minczuk,M. (2011) PDE12 removes mitochondrial RNA poly(A) tails and controls translation in human mitochondria. *Nucleic Acids Res.*, **39**, 7750–7763.
23. Borowski,L.S., Szczesny,R.J., Brzezniak,L.K. and Stepien,P.P. (2010) RNA turnover in human mitochondria: more questions than answers? *Biochim. Biophys. Acta*, **1797**, 1066–1070.
24. Zuo,Y. and Deutscher,M.P. (2001) Exoribonuclease superfamilies: structural analysis and phylogenetic distribution. *Nucleic Acids Res.*, **29**, 1017–1026.
25. Chen,H.W., Rainey,R.N., Balatoni,C.E., Dawson,D.W., Troke,J.J., Wasiak,S., Hong,J.S., McBride,H.M., Koehler,C.M., Teitell,M.A. *et al.* (2006) Mammalian polynucleotide phosphorylase is an intermembrane space RNase that maintains mitochondrial homeostasis. *Mol. Cell. Biol.*, **26**, 8475–8487.
26. Wang,G., Chen,H.W., Oktay,Y., Zhang,J., Allen,E.L., Smith,G.M., Fan,K.C., Hong,J.S., French,S.W., McCaffery,J.M. *et al.* (2010) PNPASE regulates RNA import into mitochondria. *Cell*, **142**, 456–467.
27. Sarkar,D., Leszczyniecka,M., Kang,D.C., Lebedeva,I.V., Valerie,K., Dhar,S., Pandita,T.K. and Fisher,P.B. (2003) Down-regulation of Myc as a potential target for growth arrest induced by human polynucleotide phosphorylase (hPNPaseold-35) in human melanoma cells. *J. Biol. Chem.*, **278**, 24542–24551.
28. Das,S.K., Sokhi,U.K., Bhutia,S.K., Azab,B., Su,Z.Z., Sarkar,D. and Fisher,P.B. (2010) Human polynucleotide phosphorylase selectively and preferentially degrades microRNA-221 in human melanoma cells. *Proc. Natl Acad. Sci. USA*, **107**, 11948–11953.
29. Dziembowski,A., Piwowarski,J., Hoser,R., Minczuk,M., Dmochowska,A., Siep,M., van der Spek,H., Grivell,L. and Stepien,P.P. (2003) The yeast mitochondrial degradosome. Its composition, interplay between RNA helicase and RNase activities and the role in mitochondrial RNA metabolism. *J. Biol. Chem*, **278**, 1603–1611.
30. Wang,D.D., Shu,Z., Lieser,S.A., Chen,P.L. and Lee,W.H. (2009) Human mitochondrial SUV3 and polynucleotide phosphorylase form a 330-kDa heteropentamer to cooperatively degrade double-stranded RNA with a 3′-to-5′ directionality. *J. Biol. Chem.*, **284**, 20812–20821.
31. Szczesny,R.J., Borowski,L.S., Brzezniak,L.K., Dmochowska,A., Gewartowski,K., Bartnik,E. and Stepien,P.P. (2010) Human mitochondrial RNA turnover caught in flagranti: involvement of hSuv3p helicase in RNA surveillance. *Nucleic Acids Res.*, **38**, 279–298.
32. Milligan,J.F., Groebe,D.R., Witherell,G.W. and Uhlenbeck,O.C. (1987) Oligoribonucleotide synthesis using T7 RNA polymerase and synthetic DNA templates. *Nucleic Acids Res.*, **15**, 8783–8798.
33. Katoh,T. and Suzuki,T. (2007) Specific residues at every third position of siRNA shape its efficient RNAi activity. *Nucleic Acids Res.*, **35**, e27.
34. Parrott,A.M., Walsh,M.R. and Mathews,M.B. (2007) Analysis of RNA:protein interactions in vivo: identification of RNA-binding partners of nuclear factor 90. *Methods Enzymol.*, **429**, 243–260.
35. Goshima,N., Kawamura,Y., Fukumoto,A., Miura,A., Honma,R., Satoh,R., Wakamatsu,A., Yamamoto,J., Kimura,K., Nishikawa,T. *et al.* (2008) Human protein factory for converting the transcriptome into an in vitro-expressed proteome. *Nat. Methods*, **5**, 1011–1017.
36. Temperley,R.J., Seneca,S.H., Tonska,K., Bartnik,E., Bindoff,L.A., Lightowlers,R.N. and Chrzanowska-Lightowlers,Z.M. (2003) Investigation of a pathogenic mtDNA microdeletion reveals a translation-dependent deadenylation decay pathway in human mitochondria. *Hum. Mol. Genet.*, **12**, 2341–2348.
37. Mercer,T.R., Neph,S., Dinger,M.E., Crawford,J., Smith,M.A., Shearwood,A.M., Haugen,E., Bracken,C.P., Rackham,O., Stamatoyannopoulos,J.A. *et al.* (2011) The human mitochondrial transcriptome. *Cell*, **146**, 645–658.
38. Poulsen,J.B., Andersen,K.R., Kjaer,K.H., Durand,F., Faou,P., Vestergaard,A.L., Talbo,G.H., Hoogenraad,N., Brodersen,D.E., Justesen,J. *et al.* (2011) Human 2′-phosphodiesterase localizes to

the mitochondrial matrix with a putative function in mitochondrial RNA turnover. *Nucleic Acids Res.*, **39**, 3754–3770.
39. Prikryl,J., Rojas,M., Schuster,G. and Barkan,A. (2011) Mechanism of RNA stabilization and translational activation by a pentatricopeptide repeat protein. *Proc. Natl Acad. Sci. USA*, **108**, 415–420.
40. Rackham,O., Shearwood,A.M., Mercer,T.R., Davies,S.M., Mattick,J.S. and Filipovska,A. (2011) Long noncoding RNAs are generated from the mitochondrial genome and regulated by nuclear-encoded proteins. *RNA*, **17**, 2085–2093.
41. Denslow,N.D., Michaels,G.S., Montoya,J., Attardi,G. and O'Brien,T.W. (1989) Mechanism of mRNA binding to bovine mitochondrial ribosomes. *J. Biol. Chem.*, **264**, 8328–8338.
42. Minczuk,M., He,J., Duch,A.M., Ettema,T.J., Chlebowski,A., Dzionek,K., Nijtmans,L.G., Huynen,M.A. and Holt,I.J. (2011) TEFM (c17orf42) is necessary for transcription of human mtDNA. *Nucleic Acids Res.*, **39**, 4284–4299.
43. Cline,S.D., Lodeiro,M.F., Marnett,L.J., Cameron,C.E. and Arnold,J.J. (2010) Arrest of human mitochondrial RNA polymerase transcription by the biological aldehyde adduct of DNA, M1dG. *Nucleic Acids Res.*, **38**, 7546–7557.
44. Delannoy,E., Stanley,W.A., Bond,C.S. and Small,I.D. (2007) Pentatricopeptide repeat (PPR) proteins as sequence-specificity factors in post-transcriptional processes in organelles. *Biochem. Soc. Trans.*, **35**, 1643–1647.
45. Schmitz-Linneweber,C. and Small,I. (2008) Pentatricopeptide repeat proteins: a socket set for organelle gene expression. *Trends Plant Sci.*, **13**, 663–670.
46. Liao,H.X. and Spremulli,L.L. (1989) Interaction of bovine mitochondrial ribosomes with messenger RNA. *J. Biol. Chem.*, **264**, 7518–7522.
47. Pagliarini,D.J., Calvo,S.E., Chang,B., Sheth,S.A., Vafai,S.B., Ong,S.E., Walford,G.A., Sugiana,C., Boneh,A., Chen,W.K. *et al.* (2008) A mitochondrial protein compendium elucidates complex I disease biology. *Cell*, **134**, 112–123.
48. Holzmann,J., Frank,P., Loffler,E., Bennett,K.L., Gerner,C. and Rossmanith,W. (2008) RNase P without RNA: identification and functional reconstitution of the human mitochondrial tRNA processing enzyme. *Cell*, **135**, 462–474.
49. Brzezniak,L.K., Bijata,M., Szczesny,R.J. and Stepien,P.P. (2011) Involvement of human ELAC2 gene product in 3′ end processing of mitochondrial tRNAs. *RNA Biol.*, **8**, 616–626.
50. de Narvaez,C.C. and Schaup,H.W. (1979) In vivo transcriptionally coupled assembly of Escherichia coli ribosomal subunits. *J. Mol. Biol.*, **134**, 1–22.
51. Slomovic,S. and Schuster,G. (2008) Stable PNPase RNAi silencing: its effect on the processing and adenylation of human mitochondrial RNA. *RNA*, **14**, 310–323.
52. Chang,D.D. and Clayton,D.A. (1985) Priming of human mitochondrial DNA replication occurs at the light-strand promoter. *Proc. Natl Acad. Sci. USA*, **82**, 351–355.
53. Bratic,A., Wredenberg,A., Gronke,S., Stewart,J.B., Mourier,A., Ruzzenente,B., Kukat,C., Wibom,R., Habermann,B., Partridge,L. *et al.* (2011) The bicoid stability factor controls polyadenylation and expression of specific mitochondrial mRNAs in Drosophila melanogaster. *PLoS Genet.*, **7**, e1002324.

SUPPLEMENTARY DATA

LRPPRC/SLIRP suppresses PNPase-mediated mRNA decay and promotes polyadenylation in human mitochondria

Chujo, T. et al.

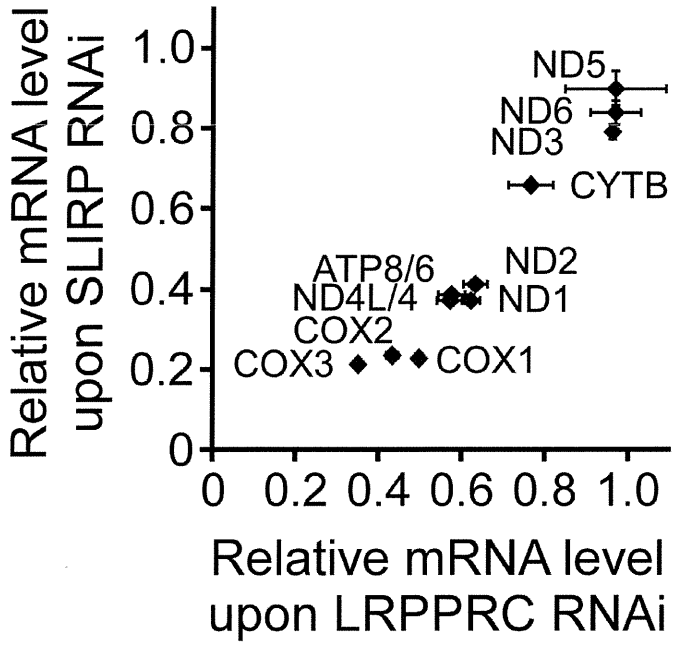

Figure S1

Correlation between relative changes in each mRNA level upon *SLIRP* knockdown (Figure 2B) and *LRPPRC* knockdown (Figure 2C).

The correlation factor (R^2) of the plot is 0.96.

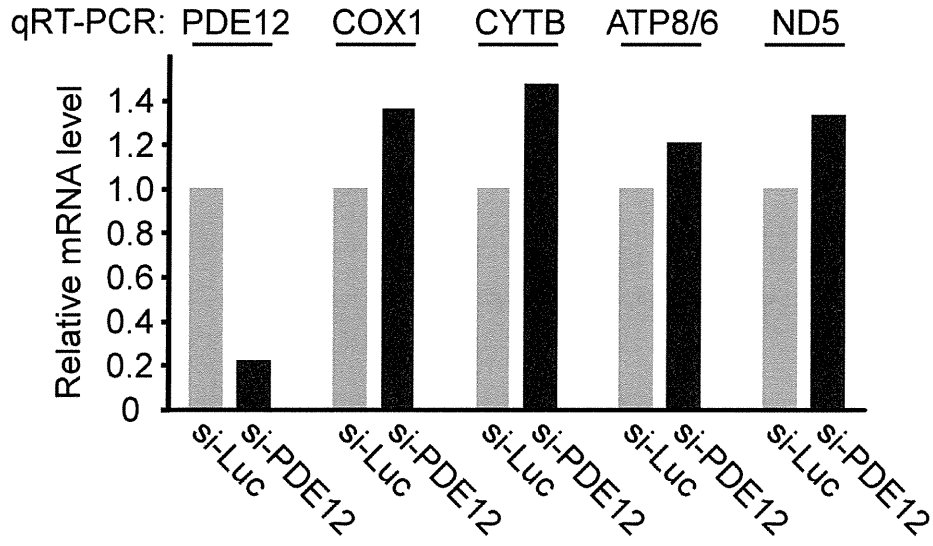

Figure S2

Relative change of mRNA levels following *PDE12* knockdown.

HeLa cells were transfected with siRNA targeted against *PDE12*. Four days after transfection, total RNA was extracted. mRNAs for *PDE12*, *COX1*, *CYTB*, *ATP8/6* and *ND5* were quantified by qRT-PCR. The relative change in each mRNA level upon *PDE12* knockdown was normalized by *GAPDH* mRNA level, and compared with that in HeLa cells transfected with siRNA targeting *luciferase* (as a control). The primers are listed in Table S1.

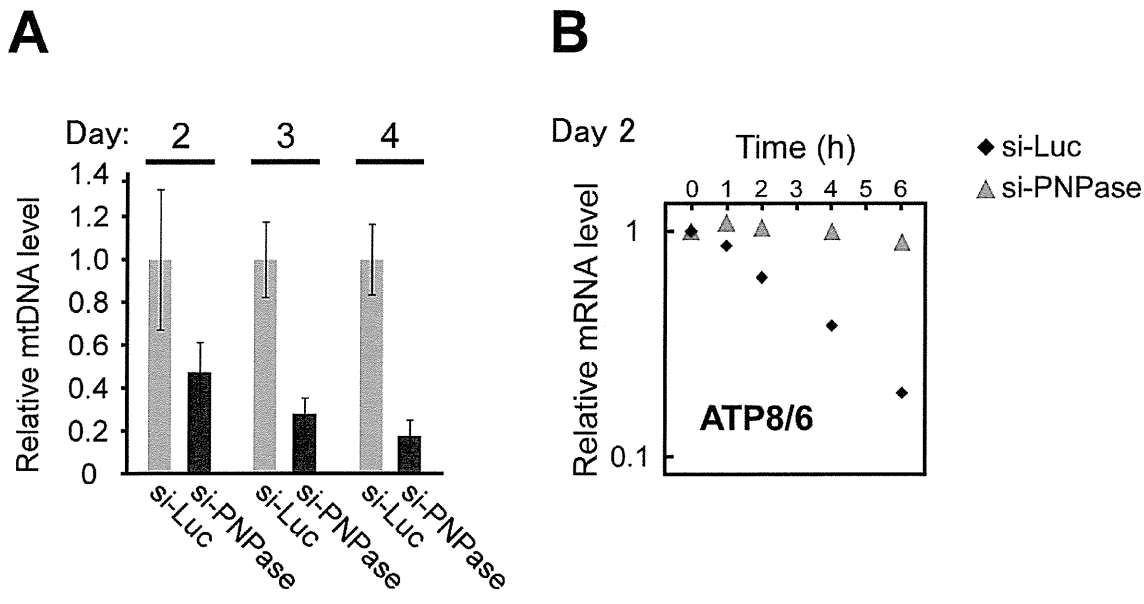

Figure S3

Effects of *PNPase* knockdown

(**A**) Relative change of mtDNA level (means ± s.d., n=3) following *PNPase* knockdown. HeLa cells were transfected with siRNA targeted against *luciferase* or *PNPase*. Two, three or four days after transfection, total DNA was extracted. mtDNA levels were analyzed by qPCR and normalized by 18S rDNA levels. The relative change in mtDNA level upon *PNPase* knockdown was compared with that in HeLa cells transfected with siRNA targeting *Luciferase*.

(**B**) Decay of *ATP8/6* mRNA in HeLa cells after two days of *PNPase* knockdown. HeLa cells were transfected with siRNA targeted against *luciferase* or *PNPase*. Two days after siRNA transfection, mitochondrial transcription was inhibited for 0, 1, 2, 4, or 6 hours, total RNA was collected, and mRNA was quantified by qRT-PCR. All data were normalized to *GAPDH* mRNA. The vertical axis represents the relative mRNA level in logarithmic scale. The steady-state level of *PNPase* mRNA decreased to 5.3% of that in the control cells upon siRNA-mediated knockdown.

OPEN ACCESS Freely available online

PLoS one

CAXII Is a Sero-Diagnostic Marker for Lung Cancer

Makoto Kobayashi[1,2], Toshihide Matsumoto[1,4], Shinichiro Ryuge[6], Kengo Yanagita[1,2], Ryo Nagashio[1,2], Yoshitaka Kawakami[3], Naoki Goshima[3], Shi-Xu Jiang[4], Makoto Saegusa[4], Akira Iyoda[5], Yukitoshi Satoh[5], Noriyuki Masuda[6], Yuichi Sato[1,2]*

1 Department of Applied Tumor Pathology, Graduate School of Medical Sciences, Kitasato University, Kanagawa, Japan, **2** Department of Molecular Diagnostics, School of Allied Health Sciences, Kitasato University, Kanagawa, Japan, **3** Biomedicinal Information Research Center, National Institute of Advanced Industrial Science and Technology, Tokyo, Japan, **4** Department of Pathology, School of Medicine, Kitasato University, Kanagawa, Japan, **5** Department of Thoracic and Cardiovascular Surgery, School of Medicine, Kitasato University, Kanagawa, Japan, **6** Department of Respiratory Medicine, School of Medicine, Kitasato University, Kanagawa, Japan

Abstract

To develop sero-diagnostic markers for lung cancer, we generated monoclonal antibodies using pulmonary adenocarcinoma (AD)-derived A549 cells as antigens by employing the random immunization method. Hybridoma supernatants were immunohistochemically screened for antibodies with AMeX-fixed and paraffin-embedded A549 cell preparations. Positive clones were monocloned twice through limiting dilutions. From the obtained monoclonal antibodies, we selected an antibody designated as KU-Lu-5 which showed intense membrane staining of A549 cells. Based on immunoprecipitation and MADLI TOF/TOF-MS analysis, this antibody was recognized as carbonic anhydrase XII (CAXII). To evaluate the utility of this antibody as a sero-diagnostic marker for lung cancer, we performed dot blot analysis with a training set consisting of sera from 70 lung cancer patients and 30 healthy controls. The CAXII expression levels were significantly higher in lung cancer patients than in healthy controls in the training set ($P<0.0001$), and the area under the curve of ROC was 0.794, with 70.0% specificity and 82.9% sensitivity. In lung cancers, expression levels of CAXII were significantly higher in patients with squamous cell carcinoma (SCC) than with AD ($P=0.035$). Furthermore, CAXII was significantly higher in well- and moderately differentiated SCCs than in poorly differentiated ones ($P=0.027$). To further confirm the utility of serum CAXII levels as a sero-diagnostic marker, an additional set consisting of sera from 26 lung cancer patients and 30 healthy controls was also investigated by dot blot analysis as a validation study. Serum CAXII levels were also significantly higher in lung cancer patients than in healthy controls in the validation set ($P=0.030$). Thus, the serum CAXII levels should be applicable markers discriminating lung cancer patients from healthy controls. To our knowledge, this is the first report providing evidence that CAXII may be a novel sero-diagnostic marker for lung cancer.

Citation: Kobayashi M, Matsumoto T, Ryuge S, Yanagita K, Nagashio R, et al. (2012) CAXII Is a Sero-Diagnostic Marker for Lung Cancer. PLoS ONE 7(3): e33952. doi:10.1371/journal.pone.0033952

Editor: Vladimir Brusic, Dana-Farber Cancer Institute, United States of America

Received September 23, 2011; **Accepted** February 20, 2012; **Published** March 16, 2012

Funding: This study was supported in part by a Grant-in-Aid for Scientific Research Council (23590414) from the Japan Society for the Promotion of Science, grants from the Third Term Comprehensive Control Research for Cancer conducted by the Ministry of Health, Labour and Welfare of Japan, as well as from the Research Project (No. 2011-1006) of the School of Allied Health Sciences, Kitasato University. The funders had no role in study design, data collection and analysis, decision to publish, or preparation of the manuscript. No additional external funding received for this study.

Competing Interests: The authors have declared that no competing interests exist.

* E-mail: yuichi@med.kitasato-u.ac.jp

Introduction

Lung cancer is the leading cause of cancer death, comprising 13% (1.6 million) of the total cancer cases and 18% (1.4 million) of the cancer deaths in the world in 2008 [1,2].

Tumor markers have been detected in sera, urine, and tissues from patients with malignant tumors, and can be used for an exact diagnosis, discrimination of benign or malignant tumors, follow-up after therapies, and prediction of the patient's outcome. At present, some sero-diagnostic markers are used for lung cancer, such as carcinoembryonic antigen (CEA) and sialyl Lewis X antigen (SLX) for adenocarcinoma (AD), and cytokeratin 19 fragment (CYFRA) and squamous cell carcinoma antigen (SCCa) for squamous cell carcinoma (SCC) [3]. The positive rates of CEA, SLX, CYFRA, and SCCa are reportedly 57, 40~50, 50~60, and 60~80%, respectively. However, it has been reported that these markers do not show sufficient tumor or organ specificities; for example, SLX can show false-positive results in the presence of pulmonary tuberculosis and pulmonary fibrosis, and CYFRA can elevate with interstitial pneumonia and renal failure.

Antibodies are usually developed using purified proteins or synthetic peptides. We have exhaustively generated monoclonal antibodies (MoAbs) against various tumor-associated proteins using the pulmonary AD-derived A549 cell as an antigen with the random immunization method [4], and over 1,000 MoAbs have been obtained [5]. This method is expected to generate antibodies against proteins with tumor-specific post-translational modifications, which are difficult to obtain by conventional immunization methods.

Carbonic anhydrase XII is a transmembrane zinc metalloenzyme that catalyzes the reversible hydration of carbon dioxide to form bicarbonate ($H_2O+CO_2 \Leftrightarrow H^+ + HCO_3^-$), and is a member of the alpha carbonic anhydrase (CA) family. CAXII has been proposed to be involved in the acidification of the extracellular microenvironment, which is suitable for rapid tumor growth. CAXII overexpression was initially detected in renal cell carcinoma, and subsequent studies confirmed its expression in

various human cancers, such as diffuse astrocytoma, breast, pancreatic, and ovarian carcinoma, as well as in non-small cell lung cancer (NSCLC) [6–11]. Its expression was influenced both by factors related to differentiation and hypoxia in breast cancer *in vivo*, and was associated with a more favorable prognosis in invasive breast carcinoma patients [12]. Higher CAXII expression was also correlated with a better overall and disease-specific survival in patients with resectable NSCLC [13]. However, no study has clarified CAXII in sera and its clinical utility as a sero-diagnostic marker for patients with malignant tumors.

In this study, the specificity of the obtained anti-CAXII antibody was confirmed by immunohistochemistry (IHC) and immunoblotting with lung cancer cell lines and lung cancer tissues. To further confirm its utility as a sero-diagnostic marker, CAXII levels in sera from patients with lung cancer were studied by dot blot analysis.

Materials and Methods

1. Cell lines

The A549 and LC-2/ad cells derived from lung AD were purchased from the Japanese Cancer Research Resources Bank (Tokyo, Japan) and RIKEN BioResource Center (Ibaraki, Japan), respectively. The RERF-LC-AI cells derived from lung SCC was purchased from the RIKEN BioResource Center. The N231 cells derived from SCLC were purchased from the American Type Culture Collection (Rockville, MD, USA). LCN1, a large cell neuroendocrine carcinoma (LCNEC) line, was established in our laboratory [14]. These cells were grown in RPMI-1640 medium (SIGMA, Steinheim, Germany) supplemented with 10% fetal bovine serum (FBS; Biowest, Miami, FL, USA), 100 units/ml of penicillin, and 100 μg/ml of streptomycin (GIBCO, Auckland, New Zealand). After harvesting and washing twice with phosphate-buffered saline without divalent ions (PBS-), sub-confluent cells were stored at −80°C for proteomics analysis or fixed in 10% formalin and embedded in paraffin for immunohistochemistry. A549 cells were also AMeX-fixed [15] for immunohistochemical screening. The SP2/O-Ag14 cells derived from a mouse myeloma were purchased from the RIKEN BioResource Center, and were grown in RPMI-1640 medium supplemented with 1× 8-azaguanine (50× Hybri-Max, SIGMA), 10% FBS, penicillin, and streptomycin.

2. Ethics statement

All samples were collected in accordance with the ethical guidelines and written consent mandated, and this study was approved by the Ethics Committee of Kitasato University School of Medicine. All patients and healthy controls were approached based on approved ethical guidelines, and those who agreed to participate in this study were required to sign consent forms. Patients could refuse entry and discontinue participation at any time. All participants provided written consent.

2.1. Sera. Sera from 70 patients with lung cancer (AD: 29, SCC: 21, SCLC: 17, and LCNEC: 3) and 30 healthy controls were used in the training set. In addition, a validation set consisting of sera from 26 patients with lung cancer (AD: 20, SCLC: 5, and LCNEC: 1) and 30 healthy controls was also studied. The clinicopathological characteristics of the patients data are summarized in Table 1.

Patient sera were collected at Kitasato University Hospital, and healthy control sera were provided by Kyowa Medex Co., Ltd. (Tokyo, Japan) and kept at −80°C until use.

3. Generation of monoclonal antibodies

A549 cell lysate was prepared with PBS(-) using an ultra-sonic homogenizer (UH-50; SMT Company, Tokyo, Japan). Five-week-old female BALB/c mice were immunized intra-peritoneally with 50 mg wet- weight of A549 cell lysate in 500 μl of PBS(-) 3 times with a two-week interval. The antibody titer was tested by IHC using 100-times diluted sera from the immunized mice as the first antibody on AMeX-fixed A549 cells. Three days prior to cell fusion, the animal with the highest titer was intra-peritoneally boosted by the same amount of A549 lysate. Hybridoma preparation and IHC screening with AMeX-fixed A549 cells were previously described [4,5].

Table 1. Clinicopathological characteristics of the patients.

Characteristics		Training set (N = 70)	Validation set (N = 26)
Age	<70	40 (57.1%)	19 (73.1%)
	≥70	30 (42.9%)	7 (26.9%)
Gender	Male	52 (74.3%)	16 (61.5%)
	Female	18 (25.7%)	10 (38.5%)
Stage	I	19 (27.2%)	17 (65.4%)
	II	11 (15.7%)	2 (7.7%)
	III	26 (37.1%)	4 (15.4%)
	IV	14 (20.0%)	3 (11.5%)
Tumor differentiation	Well	7 (13.2%)	11 (52.4%)
(NSCLC)	Moderate	10 (18.9%)	5 (23.8%)
	Poor	18 (34.0%)	4 (19.0%)
	Unknown	18 (34.0%)	1 (4.8%)
Tumor size	<3 cm	24 (34.3%)	15 (57.7%)
	≥3 cm	45 (64.3%)	6 (23.1)
	Unknown	1 (1.4%)	5 (19.2)
Nodal status	N0	23 (32.9%)	18 (69.3%)
	N1	12 (17.1%)	1 (3.8%)
	N2	23 (32.9%)	5 (19.2%)
	N3	12 (17.1%)	2 (7.7%)
Distant metastasis	M0	56 (80.0%)	23 (88.5%)
	M1	14 (20.0%)	3 (11.5%)
Histological type	AD[a]	29 (41.4%)	20 (77.0%)
	SCC[b]	21 (30.0%)	0 (0.0%)
	SCLC[c]	17 (24.3%)	5 (19.2%)
	LCNEC[d]	3 (4.3%)	1 (3.8%)

[a]Adenocarcinoma.
[b]Squamous cell carcinoma.
[c]Small cell lung carcinoma.
[d]Large cell neuroendocrine carcinoma.
doi:10.1371/journal.pone.0033952.t001

4. Proteomics analysis

4.1. Sodium dodecyl sulfate-polyacrylamide gel electrophoresis (SDS-PAGE). Proteins were extracted from each of A549, LC-2/ad, RERF-LC-AI, N231, and LCN1 cells with detergent lysis buffer [16] using an ultra-sonic homogenizer. Ten μg each of extracted proteins were boiled and separated by SDS-PAGE with 10% polyacrylamide gel at a constant current of 20 mA. After SDS-PAGE, proteins in gels were transferred to a polyvinylidene difluoride (PVDF) membrane (Millipore Corp., Billerica, MA, USA) for immunoblotting.

4.2. Immunoblotting. Blotting membranes were blocked with 0.5% casein from bovine milk (Sigma, St. Louis, MO, USA) for 30 min at RT. The membranes were then reacted with non-

diluted hybridoma supernatant for 1 hr at RT, followed by incubation with 1,000-times diluted horseradish peroxidase-conjugated rabbit anti-mouse IgG polyclonal antibody (Dako, Glostrup, Denmark) with 0.025% Casein for 45 min at RT. Finally, signals were developed using Immobilon Western HRP reagent (Millipore Corp.).

4.3. Determination of antibody isotype. To determine the isotype of the established KU-Lu-5 antibody, we used the IsoStrip™ Mouse Monoclonal Antibody Isotyping Kit (Roche Diagnostics, Mannheim, Germany) according to the manufacturer's instructions.

4.4. Immunoprecipitation. The immunoprecipitation method used in this study was previously described [17]. In brief, A549 cells were washed with PBS (-) and treated with radioimmunoprecipitation assay (RIPA) buffer containing Complete-mini EDTA-free (Roche Diagnostics) on ice for 30 min. After centrifugation at 15,000 rpm for 30 min at 4°C, the supernatant was collected and precleared with protein G sepharose (50% slurry) (GE Healthcare Bio-Sciences Corp., Piscataway, NJ, USA) at 4°C overnight. To conjugate the primary antibody, 250 μL of primary antibody (KU-Lu-5 hybridoma supernatant) and 20 μL of protein G sepharose beads suspended in RIPA buffer were incubated with mixing at 4°C overnight. After centrifugation, the antibody-sepharose conjugate and 500 μg of total cellular protein from the precleared supernatant were incubated with mixing at 4°C for 4 hrs. The immunoprecipitates were collected by centrifugation at 15,000 rpm for 5 min at 4°C. After washing four times with RIPA buffer, the supernatant was carefully removed and the pellets were resuspended in 15 μL of 1×Laemmili's buffer. Then, 15 μL of samples were boiled and separated by SDS-PAGE with 10% polyacrylamide gel. After SDS-PAGE, gels were Zn-stained with the Negative Gel Stain MS kit (Wako Pure Chemical, Tokyo, Japan) according to the manufacturer's instructions.

4.5. Identification of antigen protein. *4.5.1. In-gel digestion.* The protein spot was excised from the SDS-PAGE gel and minced to 1 mm^3, destained with destaining solution (Wako Pure Chemical), dehydrated with 100% (v/v) ACN, and dried under vacuum conditions. Tryptic digestion was performed with a minimal volume of digestion solution which contained 20 ng/μl of trypsin (Trypsin Gold, Mass Spectrometry Grade, Promega, Madison, WI, USA) and 25 mM NH_4HCO_3 for 24 hrs at 37°C. After incubation, digested protein fragments eluted in solution were collected, and gels were washed once in 5% (v/v) trifuloroacetic acid /50% (v/v) ACN and collected in the same tube.

4.5.2. Protein identification. The collected peptide fragments were analyzed using autoflex III matrix-associated laser desorption/ionization-time of flight/time of flight mass spectrometry (MALDI-TOF/TOF MS; Bruker Daltonik, Bremen, Germany). A disposable plate, spotted α-cyano-4-hydroxycinnamic acid matrix for samples, and PAC Peptide Calibstandard for calibration (Prespotted AnchorChip 96 set for Proteomics, Bruker Daltonik) were used. Peptide mass fingerprints (PMF) were measured, and then a few peaks obtained from PMF were further measured for their tandem mass spectra as parent masses. MASCOT (http://www.matrixscience.com) using the IPI Human database (93,289 sequences; 36,994,704 residues), released on 3 May, 2011 (http://www.matrixscience.com), was used to determine proteins from PMF and tandem mass data.

5. Immunoblot analysis with recombinant CAXII protein

Recombinant CAXII protein and Venus protein as a negative control with GST-tag were prepared using a wheat germ cell-free system [18]. Fourteen μg each of recombinant CAXII and Venus proteins were boiled and separated with SDS-PAGE, followed by immunoblotting with KU-Lu-5 antibody, as mentioned in 2.4.1.

6. Immunohistochemical staining

Three-μm-thick sections, made from 10% formalin-fixed and paraffin-embedded lung cancer cell lines and 37 surgically resected lung cancers (AD: 28, SCC: 9) were deparaffinized in xylene, rehydrated in a descending ethanol series, and then treated with 3% hydrogen peroxide for 20 min. After the antigen was retrieved by autoclaving in 0.01 mol/L citrate buffer (pH 6.0) with 0.1% Tween 20 at 121°C for 10 min, the sections were reacted with non-diluted KU-Lu-5 hybridoma supernatant for 16–18 hrs at room temperature (RT). After rinsing in TBS three times for 5 min each, the sections were reacted with ChemMate Envision reagent (Dako) for 30 min at RT. Finally, the sections were visualized with Stable DAB solution (Invitrogen Corp.) and counterstained with Mayer's hematoxylin.

7. Dot blot analysis

7.1. Sample preparation. *7.1.1. Removal of albumin and IgG from serum samples.* The removal of albumin and IgG from sera was performed using a ProteoExtract Albumin/IgG Removal kit (Merck, Darmstadt, Germany) according to the manufacturer's instructions. A 60-μL sample of each sera was diluted with 540 μL of binding buffer, and allowed to pass the column by gravity flow. The flow-through fraction was collected in a collection tube. To wash the column, binding buffer was allowed to pass the column by gravity flow. The flow-through fraction was collected in the same collection tube.

7.1.2. Desalting and concentration by ultrafiltration. The albumin- and IgG-depleted samples were buffer-exchanged and concentrated using 10-kDa molecular-weight cut-off ultra-filtration VIVASPIN 2 (Sartorius, Gottingen, Germany). The samples were centrifuged at 6,000×g at 4°C until less than 100 μL, and then the buffer was exchanged for PBS (-) with concentration at 6,000×g at 4°C until concentrated to less than 50 μL. The concentrated samples were adjusted to a final volume of 60 μL with PBS (-).

7.2. Dot blot analysis. One μl each of albumin- and IgG-depleted samples diluted to 1:20 with PBS(-) and mouse IgG (purified in our laboratory) for a positive control were spotted on a PVDF membrane (Millipore Corp.) using the automatic dot blot system with a 256-solid pin configuration (Kakengeneqs Inc., Chiba, Japan). Two sheets of membrane were prepared for one set of experiment. Spotted membranes were washed in TBS for 10 min, and blocked with 0.5% casein (Sigma) for 1 hr at RT. One membrane was then reacted with non-diluted KU-Lu-5 hybridoma supernatant, and the other membrane was reacted with antibody diluting solution [20-times diluted 0.5% casein with 0.1% Tween 20 added TBS (TBS-T)] for 30 min at RT. After rinsing in TBS-T 3 times for 5 min each, membranes were incubated with 1,000-times diluted horseradish peroxidase-conjugated rabbit anti-mouse IgG polyclonal antibody (Dako) for 30 min at RT. Finally, signals were developed with Immobilon Western reagent (Millipore Corp.). The data were analyzed using DotBlotChipSystem Ver. 4.0 (Dynacom Co., Ltd., Chiba, Japan). Each normalized signal was presented as the ratio of the positive intensity versus the negative background intensity.

8. Statistical analysis

Serum CAXII levels in patients with lung cancer and healthy controls were statistically analyzed using the Mann-Whitney *U*-test. Sensitivity, specificity, and predictive values were calculated with the SPBS software package (Ver. 9.42 for Windows) for each variable at a corresponding cut-off. Discriminant function analysis

was performed to classify patients in the "lung cancer" vs. "healthy control" group, according to the status of the biomarkers, using the SPBS software package. The area under the curve (AUC) and best cut-off point were calculated employing receiver operating characteristic (ROC) analysis. Results were considered significant when $P<0.05$.

Results

1. Confirmation of antibody titer in mouse sera

The antibody titer was tested by IHC with 1,000-times diluted sera of immunized mice as the first antibody on AMeX-fixed A549 cells. As a result, the sera from immunized mice contained antibodies that reacted with various components of A549 cells.

Using AMeX-fixed A549 cell preparations for the immunohistochemical screening of hybridomas, we finally established 188 MoAbs in total and a further study was performed with the KU-Lu-5 clone, which showed intense staining in A549 cells (Fig. 1 A).

2. Identification of antigen protein

In order to identify the antigen protein recognized by the KU-Lu-5 antibody, we performed IP with lysate from A549 cells. The results of IP are shown in Fig. 1 B, C. The antigenic protein was observed at roughly 40 kDa. To determine the antigenic protein recognized by KU-Lu-5 antibody, we excised and collected the spot from the Zn-stained gel, and proceeded with in-gel digestion. After analysis employing a MALDI-TOF/TOF MS and a MASCOT search, the protein was determined as isoform 2 of carbonic anhydrase XII (CAXII, accession: IPI00221392), which is composed of 343 amino acids with a predicted M.W. of 38,384 Da. The result was confirmed by immunoblot analysis with recombinant CAXII protein using KU-Lu-5 hybridoma supernatant as the first antibody (Fig. 1 D). The immunoglobulin isotype of KU-Lu-5 antibody was determined as IgG_1, κ.

3. Immunoblot analysis

Expression of CAXII was detected only in A549 cells as a roughly 40-kDa protein, and no clear band was detected in other cells used in this study (Fig. 2 A).

4. Immunohistochemical staining for CAXII

Immunohistochemically, membranous expression of CAXII was observed only in A549 cells (Fig. 2 B). Membranous staining was detected in 2 of the 28 ADs (7.1%) and in 2 of the 9 SCCs (22.2%) (Fig. 2 C, D).

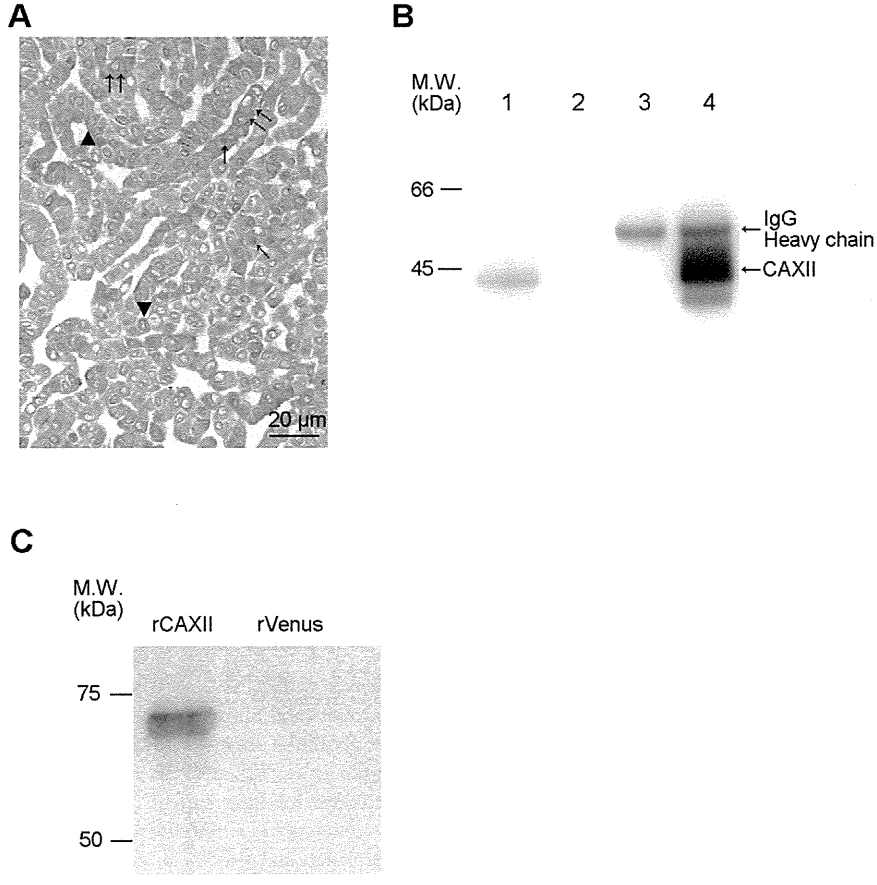

Figure 1. Production of anti-CAXII monoclonal antibody and its antigen identification. (A) The antibody titer was tested immunohistochemically using 1,000-times diluted sera of immunized mice as the first antibody on AMeX-fixed A549 cells, which were used as an immunogen. The sera of immunized mice contained antibodies that reacted with various cell components, such as the nucleus (↑), plasma membrane (▲), and cytoplasm (↑ ↑). (B) Immunoprecipitation with KU-Lu-5 antibody. Immunoblot analysis using KU-Lu-5 hybridoma supernatant as the first antibody [lane 1: A549 lysate, lane 2: A549 lysate combined with protein G, lane 3: KU-Lu-5 antibody combined with protein G, lane 4: A549 lysate combined with KU-Lu-5 antibody]. Lanes 2 to 3 are negative controls, and immunoprecipitated product with KU-Lu-5 antibody was detected in lane 4 (↑). (C) Confirmation of identified antigen protein. KU-Lu-5 antibody reacted with recombinant CAXII protein (64 kDa), but not with recombinant Venus protein.

doi:10.1371/journal.pone.0033952.g001

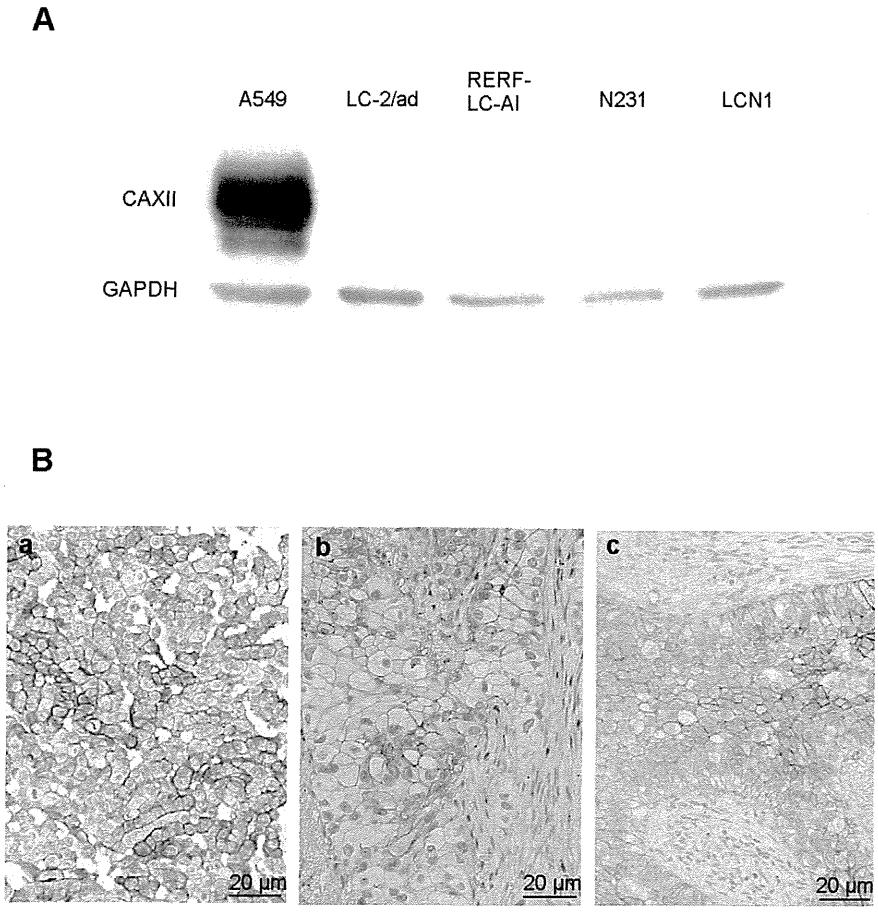

Figure 2. Expression of CAXII antibody in lung cancer cell lines and tissues. (A) Immunoblot analysis of CAXII in lung cancer cell lines. CAXII was detected as an approximately 40-kDa protein with A549 cells. (B) Immunostaining of CAXII in A549 cells (a), adenocarcinoma (b), and squamous cell carcinoma (c) of the lung, and each showed membranous staining of CAXII.
doi:10.1371/journal.pone.0033952.g002

5. Serum CAXII in patients with lung cancer

The serum CAXII levels were significantly higher in lung cancer patients than in healthy controls in the training set ($P<0.0001$). Relative values of serum CAXII levels ranged from 0.101 to 4.01 (median: 1.520) in lung cancer patients, but 0.006 to 1.679 (median: 0.290) in healthy controls (Fig. 3 A). In lung cancer, CAXII serum levels of SCC patients were significantly higher than those of AD patients ($P = 0.03$) (Fig. 3 A). The area under the ROC curve (AUC) between lung cancers and healthy controls was 0.794 (Fig. 3 B). When an optimal cut-off value of 0.387 for CAXII was applied, the diagnostic sensitivity and specificity for lung cancer were 82.9 and 70.0, respectively, and the negative and positive predictive values were 0.617 and 0.863, respectively. Furthermore, within SCCs, serum CAXII levels were significantly higher in patients with well- and moderately differentiated tumors than those with poorly differentiated ones ($P = 0.027$) (Fig. 4 A), and tended to be higher in patients with a tumor size of less than 3 cm rather than more than 3 cm ($P = 0.0538$). However, there was no difference in the smoking history of patients (Fig. 4 B). CAXII levels in stage I, II, and III ADs were 1.501, 0.704, and 1.001, respectively, and CAXII levels in stage I, II, and III SCCs were 1.764, 2.093, and 1.854, respectively. These data were summarized in Table 2. No relations between the CAXII serum levels and tumor stage or presence of metastasis were identified for either ADs or SCCs. To further confirm the utility of serum CAXII levels as a sero-diagnostic marker, 56 additional samples of sera were analyzed by dot blot analysis as a validation study. The serum CAXII levels were also significantly higher in lung cancer patients than in healthy controls in the validation set ($P = 0.030$). Relative values of serum CAXII levels ranged from 0.000 to 8.023 (median: 3.921) in lung cancer patients, but 0.000 to 8.331 (median: 2.806) in healthy controls (Fig. 5). When an optimal cut-off value of 3.086 for applied, the diagnostic sensitivity and specificity for lung cancer were 65.4 and 70.0, respectively.

Discussion

In this study, aiming to discover useful sero-diagnostic markers for lung cancer, we generated monoclonal antibodies using lung AD-derived A549 cells as antigens. From the obtained 188 antibodies, we focused on an antibody recognizing CAXII, and explored its clinical utility as a sero-diagnostic marker for lung cancer. This random immunization method is expected to yield antibodies against tumor-specific proteins with post-translational modifications, which are difficult to obtain by conventional immunization methods. Actually, several authors have reported that monoclonal antibodies generated by this method are useful as diagnostic and prognostic markers for cancers [5,17,19]. Battke *et al.* [20] established a 6A10 antibody recognizing CAXII using a similar immunization methodology. However, the obtained antibodies were limited to those only reacting with cell surface antigens because of using flow cytometry for the screening of hybridomas. In the present study, the hybridomas were immunohistochemically screened which facilitated the obtaining of